(12) INTERNATIONAL APPLICATION PUBLISHED UNDER THE PATENT COOPERATION TREATY (PCT)

(19) World Intellectual Property Organization
International Bureau

(43) International Publication Date
7 August 2014 (07.08.2014)

WIPO | PCT

(10) International Publication Number
WO 2014/120321 A2

(51) **International Patent Classification**:
B32B 27/12 (2006.01)

(21) **International Application Number**:
PCT/US2013/070110

(22) **International Filing Date**:
14 November 2013 (14.11.2013)

(25) **Filing Language**: English

(26) **Publication Language**: English

(30) **Priority Data**:
61/726,157 14 November 2012 (14.11.2012) US

(71) **Applicant**: **NDSU RESEARCH FOUNDATION** [US/US]; 1735 NDSU Research Park Drive Dept 4400, PO Box 6050, Fargo, North Dakota 58108-6050 (US).

(72) **Inventors**: **WU, Xiangfa**; 1735 NDSU Research Park Drive Dept 4400, PO Box 6050, Fargo, North Dakota 58108-6050 (US). **RAHMAN, Arifur**; 1735 NDSU Research Park Drive Dept 4400, PO Box 6050, Fargo, North Dakota 58108-6050 (US). **ZHOU, Zhengping**; 1735 NDSU Research Park Drive Dept 4400, PO Box 6050, Fargo, North Dakota 58108-6050 (US). **ZHAO, Youhao**; 1735 NDSU Research Park Drive Dept 4400, PO Box 6050, Fargo, North Dakota 58108-6050 (US).

(74) **Agents**: **COLEMAN, Kyle S.** et al.; McKee, Voorhees & Sease, P.L.C., 801 Grand Avenue, Suite 3200, Des Moines, Iowa 50309-2721 (US).

(81) **Designated States** *(unless otherwise indicated, for every kind of national protection available)*: AE, AG, AL, AM, AO, AT, AU, AZ, BA, BB, BG, BH, BN, BR, BW, BY, BZ, CA, CH, CL, CN, CO, CR, CU, CZ, DE, DK, DM, DO, DZ, EC, EE, EG, ES, FI, GB, GD, GE, GH, GM, GT, HN, HR, HU, ID, IL, IN, IR, IS, JP, KE, KG, KN, KP, KR, KZ, LA, LC, LK, LR, LS, LT, LU, LY, MA, MD, ME, MG, MK, MN, MW, MX, MY, MZ, NA, NG, NI, NO, NZ, OM, PA, PE, PG, PH, PL, PT, QA, RO, RS, RU, RW, SA, SC, SD, SE, SG, SK, SL, SM, ST, SV, SY, TH, TJ, TM, TN, TR, TT, TZ, UA, UG, US, UZ, VC, VN, ZA, ZM, ZW.

(84) **Designated States** *(unless otherwise indicated, for every kind of regional protection available)*: ARIPO (BW, GH, GM, KE, LR, LS, MW, MZ, NA, RW, SD, SL, SZ, TZ, UG, ZM, ZW), Eurasian (AM, AZ, BY, KG, KZ, RU, TJ, TM), European (AL, AT, BE, BG, CH, CY, CZ, DE, DK, EE, ES, FI, FR, GB, GR, HR, HU, IE, IS, IT, LT, LU, LV, MC, MK, MT, NL, NO, PL, PT, RO, RS, SE, SI, SK, SM, TR), OAPI (BF, BJ, CF, CG, CI, CM, GA, GN, GQ, GW, KM, ML, MR, NE, SN, TD, TG).

[Continued on next page]

(54) **Title**: SELF-HEALING NANOFIBERS, COMPOSITES AND METHODS FOR MANUFACTURING

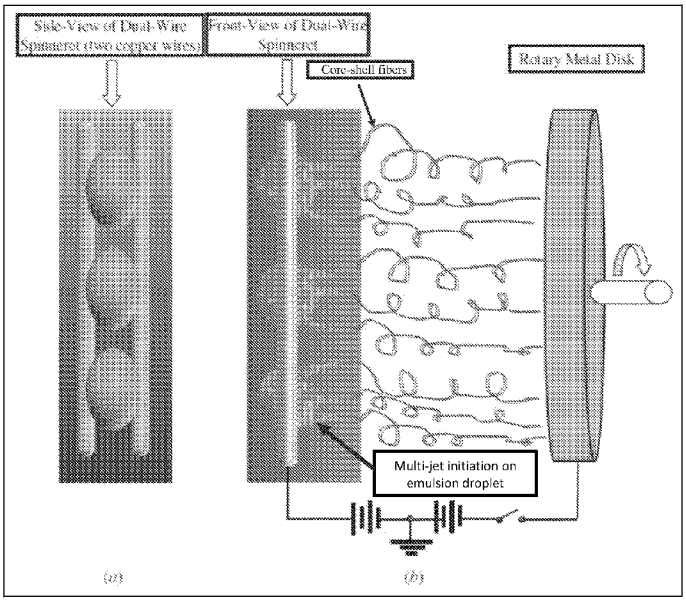

FIG. 14

(57) **Abstract**: The present invention is a new type of hybrid high-strength carbon-fiber/epoxy composites reinforced with ultrathin toughening and self-healing core-shell fibers at interfaces by means of wetted lay-up, followed by vacuum-assisted resin transfer molding (VARTM) technique. The core-shell fibers loaded with liquid healing agent (a liquid monomer at room temperature) are produced by co- electrospinning, in which a plastic polymer solution (dissolved in an organic solvent) is used as the exterior jet and the monomer solution (dissolved in the same organic solvent) is used as the interior jet. Also described is a fiber manufacturing device utilizing a novel dual-wire emulsion-electrospinning method capable of producing ultrathin continuous core-shell and hollow fibers in commercial volumes.

WO 2014/120321 A2

Published:

— *without international search report and to be republished upon receipt of that report (Rule 48.2(g))*

SELF-HEALING NANOFIBERS, COMPOSITES AND METHODS FOR MANUFACTURING

CROSS-REFERENCE TO RELATED APPLICATIONS

This application claims priority under 35 U.S.C. §119 to provisional application Serial No. 61/726,157 filed November 14, 2012, herein incorporated by reference in its entirety.

GRANT REFERENCE

This invention was made with government support under Grant No. DE-FG02-06ER46292 awarded by the Department of Energy and Grant No. 1234297 awarded by the Civil, Mechanical and Manufacturing Innovation (CMMI) Division of the National Science Foundation. The government has certain rights in the invention.

BACKGROUND OF THE INVENTION

I. Field of the Invention

The present invention relates to self-healing nanofibers, composites and methods for manufacturing the same. More specifically, but not exclusively, the present invention relates to a high-strength carbon-fiber/epoxy composite reinforced with self-healing nanofibers and methods for manufacturing the same.

II. Description of the Prior Art

After over four-decades of intensive research, advanced composites made of high-modulus fibers in compliant polymeric matrix have emerged as lightweight structural materials of choice for many aerospace and aeronautical applications because of their distinct advantages superior to traditional metallic materials including high specific strength and stiffness, excellent formability and immunity to corrosion, etc. [1-3].

For self-healing composites, it is essential to develop a feasible healant encapsulation system that is capable of protecting either the healant or the catalyst, or both, making the selection and manufacturing of effective self-healing micro-containers the first step towards a successful application of this material concept. A suitable self-healing system should be (i) easily encapsulated and ruptured; (ii) stable and reactive over the

entire service life of the polymeric components under various environmental conditions; (iii) responsive quickly to heal damage once triggered; (iv) low cost and low adverse impact on the original material properties [12]. By examining the current self-healing polymer composites, it is found that the typical size of healant containers (either microcapsules or hollow microfibers) is up to hundreds of micrometers, much larger than that of the reinforcing microfibers. Due to stress concentration, the large healant containers in brittle matrix may lead to the spots of earlier failure of the composites. Furthermore, the uniform distribution of microcapsules in resin or hollow microfibers aligned into the reinforcing microfibers may yield additional difficulties in reinforcing the local weak interfaces in fiber-reinforced polymer matrix composites ("PMCs") where localized delamination is the dominative failure mode.

Therefore, it is an object, feature, or advantage of the present invention to provide a novel interface self-healing technique for PMCs based on healant-loaded core-shell nanofibers, and a method of manufacturing the core-shell nanofibers that can be scaled to production quantities.

One or more of these and/or other objects, features or advantages of the present invention will become apparent from the specification and claims that follow.

SUMMARY OF THE INVENTION

The present invention provides self-healing nanofibers, composites and methods for manufacturing the same.

One exemplary embodiment provides a self-repairing composite. The composite may include a bulk constituent and a reinforcing constituent. The composite has one or more interfacial regions, at least one fiber having a hollow core, and one or more self-repairing agents housed in the hollow core. The hollow-core fiber may, for example, be incorporated at the one or more interfacial regions for repairing the composite.

Another embodiment provides a method for manufacturing self-repairing composites. The method includes using a fiber collector and a pair of closely spaced conductive wires comprising a dual-wire spinneret. A two-compound emulsion is delivered along the dual-wire spinneret. A voltage is applied between the dual-wire spinneret and the film collector. One or more emulsion jets are ejected from the dual-wire spinneret. A first solution is enwrapped with a second solution from the two-compound

emulsion by stretch-forming the second solution under electrostatic force into a core of the first solution.

Yet another embodiment provides a self-repairing fiber. The fiber includes a fiber shell having terminal ends. The fiber shell is formed from a two or more compound solution. A fiber core is enwrapped by the fiber shell at least between the terminal ends. The fiber core is formed from the two or more compound solution. The fiber core includes one or more self-repairing agents.

BRIEF DESCRIPTION OF THE DRAWINGS

Illustrated embodiments of the present invention are described in detail below with reference to the attached drawing figures, which are incorporated by reference herein, and where:

Fig. 1 is a pictorial representation of schematic damage modes in a cross-ply polymer composite in accordance with an illustrative embodiment;

Fig. 2 is a pictorial representation of hybrid multiscale PMC reinforced with electrospun continuous nanofibers in accordance with an illustrative embodiment;

Fig. 3 is a pictorial representation of coaxial spinneret, a coelectrospun core-shell DCPD/DMF nanofiber mat and optical micrograph of typical core-shell DCPD/DMF nanofibers in accordance with an illustrative embodiment;

Fig. 4 is a pictorial representation of a three-point bending test setup and specimens in accordance with an illustrative embodiment;

Fig. 5 is a pictorial representation of the load-displacement curves of two self-healing specimens in accordance with an illustrative embodiment;

Fig. 6 is a pictorial representation of SEM micrographs for hybrid multiscale self-healing PMCs in accordance with an illustrative embodiment;

Fig. 7 is a pictorial representation of other SEM micrographs for hybrid multiscale self-healing PMCs showing dicyclopentadiene release in accordance with an illustrative embodiment;

Fig. 8 is a pictorial representation of other SEM micrographs for hybrid multiscale self-healing PMCs showing the toughening mechanism in accordance with an illustrative embodiment;

Fig. 9 is a pictorial representation of a dual-wire emulsion-electrospinning configuration in accordance with an illustrative embodiment;

Figs. 10-12 are pictorial representations of optical images for emulsion-electrospun core-shell fibers in accordance with an illustrative embodiment;

Fig. 13 is a pictorial representation of a dual-wire spinneret in accordance with an illustrative embodiment;

Fig. 14 is a pictorial representation of another dual-wire emulsion-electrospinning configuration in accordance with an illustrative embodiment

Fig. 15 is a pictorial representation of a micrographed emulsion in accordance with an illustrative embodiment;

Fig. 16 is a pictorial representation of a dual-wire emulsion-electrospinning process in accordance with an illustrative embodiment;

Fig. 17 is a pictorial representation of micrographed core-shell fibers in accordance with an illustrative embodiment;

Fig. 18 is a pictorial representation of FT-IR spectra for core-shell nanofibers in accordance with an illustrative embodiment;

Fig. 19 is a pictorial representation of micrographed emulsion-electrospun core-shell fibers in accordance with an illustrative embodiment; and

Fig. 20 is another pictorial representation of micrographed emulsion-electrospun core-shell fibers in accordance with an illustrative embodiment.

DETAILED DESCRIPTION OF THE PREFERRED EMBODIMENTS

First developed for military aircraft applications in 1970s, advanced composites now play a crucial role in a broad range of current generation military aerospace systems, resulting in weight saving of 10-60% over metal design, with 20- 30% being typical as achieved by the U.S. Air Force B2 bomber and recent F-22 raptor (24%). Commercial transport aviation has also witnessed a significant increase in adoption of polymer composites during the past decades; the new Boeing 787 Dreamliner is made from 50% polymer composites by weight and more than 50% by volume. Recently, with the eager demand for faster, more agile and more mobile ground vehicles in the U.S. military operations [4] and the growing concern of cost savings and fuel efficiency in civil vehicles, polymer composites have also been finding rapidly growing applications in lightweight

armors, ground vehicles, etc. Yet, there continue to be barriers and challenges to the expanded exploitation of composites technology for primary transport structures such as wing and fuselage in aircrafts and composite propulsion shaft in heavy duty ground vehicles. These include damage tolerance, fuel containment, lightening protection, repair and nondestructive inspection, modeling and failure prediction, cost-effective manufacturing, etc. [5]. Beyond these, advanced composites with self-healing function are particularly attractive. For example, if an antenna of the space station was made of self-healing composites, it could be possible to save huge maintenance cost associated with space walks and shuttle launches. To date, most research in advanced composites has been mainly focused on further exploitation of the existing properties of these materials to satisfy ever growing aggressive structural requirements, while relatively less has been aimed at exploration of innovative material functions including damage self-repairing and stiffness/strength self-recovery to mimic biological functions. In nature, biological bodies' ability to heal (e.g., bleeding, blood clotting, tissue bruising, tree bark compartmentalization healing, etc.) has inspired several self-healing mechanisms that can be tempting to be used in engineering materials [6]. Yet, these biological self-healing mechanisms are usually too complicated to be directly mimicked for use in engineering materials. Thus, materials scientists and engineers have formulated several simplified material healing concepts that offer the capability of restoring the mechanical performance of materials [6-14]. For polymer composite materials PMCs, two basic self-healing mechanisms to mimic mammal bleeding have been broadly studied in recent years, in which the self-healing chemistry is based on living ring-opening metathesis polymerization (ROMP) [15]. The first self-healing system is based on the microencapsulation approach in which microcapsules containing liquid healing agent (healant) and polymeric resin containing catalyst form the constitutive phases of the composite [7,16-25]; the second is based on hollow microfibers containing healing agent [26-33]. In principle, each self-healing strategy involves incorporation of a healant microcontainer (either microcapsule or hollow microfiber) and a dispersed catalyst within the polymeric resin. Upon cracking, the wall of the microcontainers (typically with waxy walls) can be ruptured by the propagating crack front, which results in the release of healant into the crack through capillary action. Subsequent ROMP of the healant under initiation of the embedded catalyst heals the microcracks and prevents further crack growth. To date, the mostly studied self-healing

system for PMCs is made up with the ROMP of dicyclopentadiene (DCPD, $C_{10}H_{12}$) and Grubbs' catalyst. The synthesis and characterization of the Grubbs' catalysts has been extensively investigated [15]. The DCPD/Grubbs' catalyst system could provide a number of advantages such as a long shelf life, low monomer viscosity and volatility, completion of polymerization at ambient condition in several minutes, low shrinkage upon polymerization, and formation of a tough and highly cross-linked crack filling material [7,10]. In addition, healing based on ROMP of DCPD/Grubbs' catalyst may form living poly-(DCPD) chain ends capable of continuously growing with the addition of more monomers. If a new monomer is supplied at any time to the end of the chain, further ROMP occurs and the chain extends making it possible to achieve multiple healings simply through replenishing the supply of the DCPD monomer.

I. Nanofiber-Based Interface Toughening and Self-Healing Method for Fiber-Reinforced Polymer Composite Materials ("PMCs")

In principle, the strength of PMCs results from a combined effect of the strength and toughness of the material constituents (i.e., the reinforcing fibers and polymeric matrix), fiber/matrix interfacial properties, microstructure of the composite (e.g., fiber alignment, ply layup, fiber volume fraction, etc.), dominative failure modes, etc. Subjected to external loading, the failure process of a fiber-reinforced PMC laminate is typically a progressive avalanche consisting of microcrack nucleation, matrix cracking, fiber breakage, fiber and matrix debonding, delamination, and final catastrophic failure. The typical damage modes in a cross-ply fiber- reinforced PMC laminate are illustrated in Fig. 1. The actual failure process of a PMC is much more complicated, highly depending upon the types of load, fiber and ply architecture, and physical properties of the constituents, among others.

In reality, given a fiber/matrix combination, a pragmatic toughening technique adoptable to enhance the strength and toughness of a PMC needs to address and resolve one or several failure modes at an affordable cost. To date, several effective toughening techniques and concepts have been formulated and implemented in PMCs such as free-edge delamination-suppression designs [3], laminate stitching [34], modification of matrix resins by incorporation of rigid/rubbery micro and nanoparticles [35,36], controlled fiber debonding and fiber surface treatment [37], and interleaving [38]. Among these, the free-edge delamination-suppression concepts (e.g., edge reinforcement and edge modification)

are rooted in altering the singular free-edge stresses near laminate edges [3, 39, 40], while interleaving is based on incorporating discrete thin interlayers of tough plastic resin, particulates, whiskers, or microfibers into the interlaminar regions and therefore enhances the interlaminar fracture toughness, especially in the cases of mode II shearing and impact. Recently, by utilizing the advantages of the above interface toughening techniques and the progress in fabrication of continuous nanofibers, an innovative delamination suppression scheme for PMC laminates has been proposed which is based on incorporation of discrete, ultrathin fibers at ply interfaces [41-43]. The resulted hybrid multiscale PMC is shown in Fig. 2. The continuous ultrathin reinforcing fibers can be tough plastic polymer nanofibers produced by solution electrospinning [44-49], glass nanofibers [50] by melt electrospinning, or their derivatives such as carbonized polymer nanofibers [51, 52]. Experimental studies have indicated that electrospun polymer (PAN), glass nanofibers (SiO2), and carbon nanofibers with as-electrospun PAN nanofibers as precursor can noticeably increase the delamination toughness (20~50%) and the out-of-plane shear strength in a wide range of loading rates [49,50-52], especially in the extension of the fatigue life cycles of angle-ply PMCs [49]. The toughening mechanisms of these nanofibers at the interfaces of PMCs include improvement of interlaminar fracture toughness and suppression of singular stresses near laminate free-edges since the entangled nanofibers at ply interfaces behave much like the hooks and loops in Velcro [41]. The main advantages of this interface toughening technique include low-weight penalty (<1% in volume fraction), low nanofiber content, and low impact to the processing and global properties of the composite (e.g., specific stiffness, volume fraction of the reinforcing fibers, etc.). Therefore, this toughening technique can be easily integrated into conventional composites fabrication process. Yet, similar to other interface toughening techniques, this interface toughening scheme does not carry any self-repairing functionality. In fact, the mechanical properties of PMCs reinforced with such nanofibers at ply surfaces will still irreversibly degrade with time. Thus, a desirable interface toughening strategy advanced PMCs is expected being capable of both toughening and self-healing.

In order to incorporate the innovative self-healing function into fiber-reinforced structural PMCs, especially at the weak interfaces, while keeping the unique advantages of the novel nanofiber-based interface toughening concept [41,49], novel liquid healant-

loaded nonwoven core-shell nanofibers are produced by using a low-cost coelectrospinning technique developed recently [53-55] to replace the aforementioned ultrathin nanofibers at ply interfaces (See Fig. 2). Thus, similar to the process of fabricating hybrid multiscale PMCs, after curing, the healant-loaded core-shell nanofibers can be entangled into the resin-rich interlayers (with the thickness of tens of microns) between neighboring plies forming ultrathin toughening and self-healing interlayers. In principle, before scission, these core-shell nanofibers are expected to function as toughening nanofibers [41,49]; moreover, once nanofiber scission happens due to crack-opening and fiber stretching and pull-out induced breakage, the liquid healant will release autonomically at crack fronts under the action of capillary force and then heal the cracks, i.e. result in interfacial self-healing. Detailed description of fabrication of healant-loaded core-shell nanofibers and processing of self-healing PMCs as well as characterization of the self-healing effect will be addressed in the following sections. The present disclosure further contemplates that the liquid healant may vary in viscosity based on ambient conditions. Additives or other considerations are contemplated to allow the liquid healant to flow regardless of the ambient conditions (e.g., cold temperatures). It is also contemplated that the liquid healant may be semi-liquid or have a higher viscosity, including the liquid healant being a gel, wax or other like-viscosity healant.

a. Experimental: Coelectrospinning of Healant-Loaded Core-Shell Nanofibers

The chemicals of PAN powder (Mw= 150,000 g/mol) and N,N-dimethylformamide (DMF, 99%) were purchased from Sigma-Aldrich Co. (St. Louis, MO) without further purification. For coelectrospinning, a solution of 10 wt% PAN in DMF was prepared to generate the PAN shell material and a solution of 10 wt% DCPD in DMF was prepared to generate the liquid DCPD core. The PAN/DMF solution was prepared by dissolving PAN powder in DMF using a magnetic stirrer installed with a hotplate; the PAN/DMF mixture had been stirred at 80°C for 6 h to form a well-electrospinnable solution. The DCPD/DFM solution was made by dissolving liquid DCPD in DMF using a magnetic stirrer at room temperature. During the coelectrospinning process, a lab-made coaxial spinneret as shown in Fig. 3(a) was used, which is made up with two coaxially assembled nozzles, pressing plate 1, tightening screws 2, upper nut 3, master tube 4, lower nut 5, seal rube ring 6, and outer nozzle 7 coaxially assembled with the inner nozzle (upper). The outer nozzle has its

inner diameter of 0.97 mm, and the inner one carries its outer and inner diameters as 0.71 mm and 0.48 mm, respectively. The PAN/DMF and DCPD/DMF solutions were placed in two 10-ml syringes and connected to the outer and inner nozzles of the coaxial spinneret, respectively. The flow rates of solutions in the outer and inner nozzles were controlled by using two digital syringe pumps (Fisher Scientific Inc., Pittsburgh, PA) such that the flow rate of the outer nozzle (PAN/DMF) was 1.5 ml/h and the flow rate of the inner one (DCPD/DMF) was 1.0 ml/h. A distance of ~25 cm was fixed between the spinneret outlet and the nanofiber collector, which was a disk-like aluminum plate and electrically grounded. A high DC voltage ~18 kV was applied between the spinneret outlet and the nanofiber collector via a positive high-voltage DC power supply (Gamma High Voltage Research, Inc., Ormond Beach, FL). A robust coelectrospinning process could be maintained via tuning the process parameters (e.g., applied DC voltage, flow rates, and distance between the nozzle outlet and nanofiber collector) around the values aforementioned. In addition, an optical microscope (IX 71 Olympus) was utilized to characterize the as-coelectrospun fibers. Figure 3(b) shows the typical continuous core-shell nanofibers loaded with liquid DCPD as the core material. By adjusting the nanofiber collection time, the thickness of the nonwoven healant-loaded core-shell nanofiber mat can be altered. In this study, the nanofiber collection time was fixed at 40 min for maximization of the interfacial toughening effect according to our recent study [49].

b. Processing of Hybrid Multi-Scale Self-Healing PMCs and Self-Healing Characterization

Commercially available UD carbon-fiber/epoxy prepregs [49] and woven carbon fabric/epoxy [50-52] have been investigated for producing hybrid multi-scale carbon-fiber/epoxy composites reinforced with PAN and carbonized electrospun PAN nanofibers, respectively, at interfaces in recent studies. The former was based on the prepreg layup molding with the aid of a vacuum bag in a hot-press; the latter was based on vacuum assisted resin transfer molding (VARTM) technique. In this study, wet layup followed by VARTM technique was employed to process the novel hybrid multi-scale self-healing PMCs, in which wet layup method would ensure the uniform wetting of the nano/microfiber fabrics into resin.

During the process, Epon 862 epoxy resin and Epicure 3234 curing agent were selected as the polymeric matrix for processing the novel PMC in the present work [56].

This resin system was purchased from Miller-Stephenson Chemical Company, Inc. (Morton Grove, IL). The mix ratio of Epon 862 and Epicure 3234 was 100/14 by weight according to the manufacturer's data sheet; a tiny quantity of Grubbs' catalyst (~0.1 g) was added into the resin (~20 g) during stirring to produce the composite panel for this study. The reinforcing UD carbon fabrics (9.0 oz/yd2) and cross-woven carbon fabrics (5.7 oz/yd2) were purchased from Fibre Glast Development Corp. (Brookville, OH). An eight-ply quasi-isotropic composite laminate with a [0o/±45o/90o]S stacking sequence was manufactured, in which the 0o and 90o plies were based on UD carbon fabrics and the +45o and -45o plies are based on cross-woven carbon fabrics. The self-healing core-shell nanofiber mats were placed locally at the interfaces of 0o/45o and 45o/90o, respectively, where out-of-plane interfacial shear failure (delamination) was expected based on a free-edge stress calculation [49,57]. Wet layup followed by VARTM was utilized for processing of the self-healing PMC panel. Vacuum pressure of 27 mm Hg had been maintained during the initial curing at room temperature for 24 hrs. The obtained composite panel had been further post-cured in an oven (1 hr at 100 C) before the mechanical test for self-healing evaluation.

For the purpose of the mechanical characterization of the self-healing specimens, the PMC specimens with dimensions: ~100 mm×20mm×2.35 mm were cut from the above post-curved PMC laminate (5"×5"×0.1") using a diamond-tipped rotary saw installed with a water cooling system. Edges of the machined specimens were polished manually using sandpaper to avoid possible pre-damage during the test. Three-point bending test (ASTM-D790) was selected to characterize the flexural stiffness of the novel hybrid multi-scale PMC specimens reinforced with self-healing core-shell nanofibers at interfaces on an Instron machine. Figure 4 shows the three-point bending test setup, in which the span between the two supporting pins was fixed at 75 mm. All the mechanical tests were performed at room temperature with a displacement-control mode such that the loading rate of 5 mm/min was applied. In this study, five specimens were used for evaluation of the self-healing effect in the flexural stiffness recovery after first-ply pre-damage.

With the three-point bending test setup (Figure 4), pre-damage test was first performed by loading the self-healing composite specimens at a constant crosshead speed of 5 mm/min until the first-ply failure happened. Then, the test was stopped and the specimen was unloaded immediately and removed from the testing frame. To simplify the

self-healing process for comparison, four specimens after the pre-damage test were heated in a hot press at 100oC for 1 hr. One specimen was kept as it was after the pre-damage test. Then, all the pre-damaged specimens were post-tested at room temperature using the same testing procedure and control parameters mentioned above. Thus, for each specimen, two load-displacement curves can be gained and recorded corresponding to the first-ply failure test and post three-point bending test. Typical failed portions of the specimens were sampled and coated with an ultrathin carbon (a few nanometers by estimation) by using a sputter, which were used for fractographical analysis and exploration of the potential toughening and self-healing mechanisms of the core-shell nanofibers by using a JEOL 6000 JSM 6300V SEM.

c. Experimental Results and Toughening and Self-Healing Mechanisms

Introduced here is the recovery rate of the initial flexural stiffness of the self-healing PMC laminates for quantitative evaluation of the healing efficiency of the interfacial self-healing method. The stiffness recovery rate can be defined as:

$$Stiffness\ Recovery\ Rate = \frac{Healed\ Flexural\ Stiffness}{Initial\ Flexural\ Stiffness} x\ 100\% \qquad (1)$$

In the above, the initial flexural stiffness is the one of a virgin self-healing PMC specimen subjected to three-point bending load; the healed flexural stiffness is the one of a pre-damaged specimen after first-ply failure, self-healing and then being reloaded in three-point bending test. It is acknowledged that first-ply failure of an angle-ply laminate is due mainly to delamination failure, thus breakage of the healant-loaded core-shell nanofibers at interfaces would release liquid DCPD, which polymerized and healed the interfacial cracks once being triggered by the Grubbs' catalyst in resin. The experimental results of the initial flexural stiffness, residual flexural stiffness after first-ply failure, healed flexural stiffness, and the stiffness recovery rate were tabulated in Table 1. Except for one specimen (due to mis-operation induced pre-damage), all the other samples exhibited clear self-healing effect. The stiffness recovery rate of the self-healing PMC specimens is up to 70% to 100%, and the healed flexural stiffness is up to 150% to 300% of the flexural stiffness of the PMC specimens after first-ply failure. It needs to be mentioned that in the preliminary study, the duration for self-healing (time between pre-damage test and post-damage test) of

the PMCs was ~2 hours. Thus, the present study indicates that liquid healant-loaded core-shell nanofibers at ply interface carry excellent self-healing effect on the flexural stiffness of the PMC laminates.

Figure 5 shows the load-displacement curves of two typical self-healing specimens subjected to pre-and post-damage three-point bending loads, respectively. From Fig. 5, it can be founded that the pre-damage load-displacement curves [the solid curves in Figs. 5(a) and 5(b)] corresponding to the first-ply failure are similar to those of common thermosetting carbon-fiber/epoxy PMCs. However, after self-healing of the pre-damaged self-healing PMC specimens, the post-damage load-displacement curves [the dashed curves in Figs. 5(a) and 5(b)] exhibit unique features closely related to the self-healing process. For instance, the post-damage tests indicated the nearly complete recovery of the initial flexural stiffness; the healed flexural stiffness was much higher than the residual one after first-ply failure. Furthermore, the healed flexural strength as showed in Fig. 5(a) could reach the flexural strength of the virgin specimen, which is double the residual flexural strength of the pre-damaged specimen after first-ply failure; in Fig. 5(b), the healed flexural strength is ~30% higher than the residual flexural strength of the pre-damaged specimen after the first-ply failure though the healed flexural strength is lower than that of the virgin specimen. The latter might be induced by the breakage of the reinforcing carbon fibers in the 0o-plies due to the large deflection at the moment of first-ply failure. Moreover, Fig. 5(b) also indicates that after self-healing, the healed PMC specimen exhibited ductile behavior that could be correlated to the plastic behavior of polymerized DCPD at the healed interfaces. Such interfacial plastic behavior expects to substantially enhance the interlaminar fracture toughness of the self-healing PMC laminates.

Sample No.	Initial stiffness (E_0) (kN/m)	Stiffness after failure (E_f) (kN/m)	Stiffness after healing (E_h) (kN/m)	Stiffness recovery rate (%)
1	163.9	61.2	159.0	97.0
2	144.8	74.5	99.0	68.3
3	145.5	46.3	150.5	103.4
4	49.0	22.8	35.3	72.0
5	120.5	44.0	36.8	30.5

Table 1. Experimental results of three-point bending tests and healing efficiency of the self-healing PMC specimens in terms of stiffness recovery rate.

Moreover, SEM-based fractographical analysis was performed to explore the potential toughening and self-healing mechanisms of the unique core-shell nanofibers at ply interfaces. During this process, SEM samples of the self-healing PMC specimens after post three-point bending test were cut from delaminated plies using a sharp scissor and coated with ultrathin carbon films of a few nanometers by using a sputter. Figure 6 shows the typical fracture surfaces. It can be clearly observed that when the core-shell nanofibers were scissored at interfaces due to crack initiation and opening, the liquid DCPD released autonomically at crack surfaces. Once touching the matrix resin containing the Grubb's catalyst, the liquid DCPD polymerized and solidified instantaneously to seal the crack surfaces, similar to discrete stitching pins. Figs. 6(a) and 6(b) also show the typical core-shell nanofiber networks full of liquid healant at ply interfaces, where the circled regions clearly indicate the spots where healant released out of the ruptured core-shell nanofibers and solidified. Figs. 6(c) and 6(d) showed zoomed regions where the DCPD healant was delivered, polymerized, and finally fractured to form the newborn crack surfaces in the post three-point bending test. The surface morphology of the newborn crack surfaces including matrix hackles and scalloped features indicates the existence of ductile interfacial failure during the post-test as expected. Some additional morphologies associated with healant release from core-shell fibers on the scale of an individual fiber are depicted in the SEM micrograph in Fig. 7. It can be seen that under pressure DCPD is squeezed from the core, and Fig. 7 (c) shows that squeezing resulted in a crack in the shell.

Besides, as shown in Fig. 8, the healant-loaded core-shell nanofibers can also function to toughen the polymer matrix simultaneously via nanofiber bridging, pull-out, breakage, etc., similar to the toughening mechanisms of solid nanofibers produced by electrospinning as explored in recent studies of interfacial toughening [49-52].

In addition, by comparison with recently developed self-healing techniques such as those based on micro/nanocapsules and hollow glass microfibers, the present self-healing technique has its merits. First, encapsulation of the healing agent to form core-shell nanofibers is based on the low-cost coelectrospinning technique. This process can be conveniently tailored via adjusting the process and material parameters for well uniform fiber diameter and optimized thickness of the nanofiber mats. This technique can also be scaled up for stable and mass production. Note also, that in addition to coelectrospinning, several other cost-effective techniques are contemplated for encapsulation of healing

agents into nanofibers and nanotubes via emulsion electrospinning, solution blowing and self-sustained diffusion [55]. Second, the present core-shell nanofibers carry the diameters nearly two orders smaller than those based on microcapsules and hollow microfibers as reported recently in the literature [7,16-18,26-28], thus the present self-healing technique can be utilized specifically for localized interfacial toughening and self-healing within a few micrometers, particularly useful to advanced aerospace and aeronautical PMCs which intrinsically bear the weak resin-rich interlayers with the thickness of tens of micrometers. In the case where the term "nano" is used herein, the present disclosure contemplates that such may be interpreted to mean measurements less than one micrometer, or less than 100nm, or less than a few hundred nanometers. An ultrathin fiber as discussed herein may include measurements (such as, for example a diameter) in the nanometer and micrometer ranges. For these PMCs, interfacial toughening and self-healing based on a tiny quantity of continuous core-shell nanofibers at interfaces will not result in an obvious weight penalty and decrease of the superior specific stiffness and strength. Third, due to their continuity, core-shell nanofibers can be easily scissored at any location once cracking happens. In contrast, nanocapsules are difficult to rupture by crack fronts; also, the low volume of healant stored in localized nanocapsules, difficult control of fabrication (generally in a wide range of size distribution) and requirement of a uniform mixture may project some additional limitations on use of micro/nanocapsules in self-healing practice. Lastly, continuous core-shell nanofiber mats can be easily sandwiched between prepregs or fiber fabrics, thus the present toughening and self-healing technique can be conveniently merged into the process of traditional PMCs manufacturing. In short, the present study opens up an innovative route for efficient interfacial toughening and self-healing techniques for advanced PMCs and other advance composites. Nevertheless, as a new cutting-edge self-healing technique, several outstanding materials science and technical issues still need resolving such as choice of proper shell material, controlled deposition of catalyst at interfaces, effect of fiber size and core/shell aspect ratio, and effect of temperature, loading rate and failure modes, etc.

d. Conclusion

In this study, a new type of hybrid multi-scale high-strength carbon-fiber/epoxy composites reinforced with core-shell self-healing nanofibers at interfaces has been proposed and successfully fabricated and characterized. The unique healant-loaded

ultrathin core-shell nanofibers were fabricated by means of the low-cost, top-down coelectrospinning technique. The present interfacial toughening and self- healing technique has extended the functionality of the recently developed nanofiber-based interfacial toughening technique for PMC laminates, where suppression of interfacial fracture (delamination) is still a challenge. The present technique has a very low weight penalty (<1% in volume fraction), very low nanofiber content, and very low impact to the processing and global specific properties of the composite. Thus, this novel interfacial toughening and self-healing technique has a promising future and is expected very useful for developing high-strength, high-toughness, self-healing lightweight PMCs for advanced structural applications in aerospace, aeronautical, and ground vehicles, among others.

II. Dual-Wire Emulsion-Electrospinning for Mass Production of Ultrathin Core-Shell and Hollow Fibers

The present invention also comprises a fiber manufacturing device capable of producing ultrathin continuous core-shell and hollow fibers with a productivity tens to hundreds of times those of existing manufacturing techniques such as coaxial-spinneret based co-electrospinning [58-63] and single-spinneret based emulsion electrospinning [61,62,64]. The innovative design of the new device includes two closely spaced parallel thin conductive wires as a spinneret (a dual-wire spinneret) for delivery of two-polymer emulsions (two immiscible polymers dissolved in an organic solvent or similar aqueous two-compound emulsion) along the dual-wire spinneret (See Fig. 9) [65-68]. The preparation of the electrospinnable two-polymer emulsion is similar to those used in regular emulsion electrospinning [61,62,64]. When a high DC voltage is applied between the dual- wire spinneret (connected to the positive electrode) and the fiber collector (connected to the negative electrode), the electrocapillary effect destabilizes the liquid held between the two parallel wires of the dual-wire spinneret and a conventional Taylor cone (well known to one skilled in the art) cannot be well developed due to the disturbed surface morphology, thus allowing multiple jets to form and eject from the destabilizing droplets on the dual-wire spinneret. In each emulsion jet, one polymer solution enwraps the droplets of the second polymer solution droplets, which depends on the thermodynamics (e.g., the free and surface energy) of the two polymer solutions in the emulsion. After vigorous jet stretching in the electrostatic field, the droplets of the second polymer solution are

deformed and stretched significantly to form the core material. After solvent evaporation, the jets deposit on the collector as an ultrathin core-shell fiber mat (see Figs. 10-12).

Sample	Copper wire diameter	Dual-wire spacing	PAN/IPDI (mass ratio)	Average diameter (OD)	Average diameter (ID)
1 (two)	0.28 mm	0.30 mm	1:1	1.60 μm	0.41 μm
2 (one)	0.28 mm	0 mm	1:1	1.95 μm	0.72 μm
3 (two)	0.78 mm	0.30 mm	1:1	2.02 μm	0.78 μm

Table 2: Experimental results of prototype two-wire emulsion-electrospinning.

Potential of spinneret	+25 kV	
Potential of fiber collector	-20 kV	
Distance from spinneret to fiber collector	25 cm	
	PAN/DMF	IPDI/DMF
Concentration (Wt. %)	10%	10%
Optical Microscope		
IX 71 Olympus, Dimension: 1392×1040		
Objective magnification 40X		

Table 3: Process parameters of coaxial fibers (PAN: polyacrylonitrile (shell polymer); IPDI: isophorone diisocyanate (core polymer, liquid at room temperature) DMF:N,N-dimethyl formamide (solvent)

III. Mass Production of Core-Shell Nanofibers via Dual-Wire Emulsion Electrospinning

Continuous nanofibers of polymers, carbon, metal oxides, etc. produced by the low-cost top-down electrospinning technique [69] represent a new class of one-dimensional (1D) nanostructured materials that have found extensive applications in protective clothing and wound dressing, [70] filtration, [71] nanofiber composites, [72] scaffolds for tissue growth, [73] drug delivery, [74] energy harvesting, conversion and storage, [75] etc. Electrospinning has also been extended to produce core-shell and hollow nanofibers based on a coaxial spinneret, i.e., coelectrospinning, [76] in which two polymer solutions are utilized to form the core and shell materials, respectively. In addition, coelectrospun core-shell nanofibers can be further converted into hollow nanofibers via extracting or thermal decomposition of the core material. [76b] Continuous core-shell and hollow nanofibers can

be potentially used for gas and liquid transport, drug delivery, electrode materials of supercapacitors and rechargeable batteries, and encapsulation of healing agent for self-healing composites, [77] etc. In addition, core-shell nanofibers can also be produced by means of emulsion electrospinning. [78] During the process, the core and shell materials are first dissolved separately into solvent to form two immiscible or less miscible solutions. Proper mixture of the two solutions leads to an electrospinnable emulsion. Upon electrospinning of the emulsion, droplets of one solution are encapsulated into the electrospinning jet, which are further deformed, elongated, and consequently formed the core of the core-shell fiber. Therefore, emulsion electrospinning can be utilized for producing a variety of core-shell and hollow nanofibers based on the conventional electrospinning setup with a single spinneret, while proper preparation of an electrospinnable emulsion is required.

Yet, similar to the conventional needle-based electrospinning process, the productivity of coelectrospinning and emulsion electrospinning is very low, largely a few grams per day, which could not satisfy the requirement of practical biomedical and industrial applications. To date, increasing research effort has been devoted to enhancing the manufacturing productivity of core-shell nanofibers such as utilizing destabilization of two thin immiscible polymer solution layers based on the principle of needleless electrospinning, [79] i.e., free-surface electrohydrodynamic jetting. However, such a technical approach may encounter the difficulties in view of electrohydrodynamic theory since initiation of multiple jets from a thin dielectric liquid film depends upon its electrohydrodynamic destabilization in electrostatic field. The wavelength of such an electrohydrodynamic destabilization highly relies on the surface (interface) tension, dielectric constant, mass density, and thickness of the thin liquid film. [79c,d] Thus, it is challenging to tune the parameters of the two liquid films (e.g., thickness) such that simultaneous destabilization of two immiscible liquid films with very close wavelengths is guaranteed for generating stable core-shell jets. There may exist the possibility of initiating the jets due only to the destabilization of the top or bottom liquid layer, however, in such a case the second liquid film actually works to stabilize the liquid films, i.e., suppression of free-surface jetting. Therefore, novel technique for mass production of ultrathin core-shell fibers is still desired in order to satisfy the ever growing need of core-shell fibers in broad industrial sectors.

A novel dual-wire emulsion-electrospinning method for massive production of ultrathin core-shell polymer fibers is contemplated, in which the emulsion made of one polymer solution droplets merged in the second polymer solution can be delivered via thin liquid film between two closely positioned wires as spinneret (coined as dual-wire spinneret as shown in Fig. 13).[80] After destabilization of the thin emulsion film due to external force such as the electrostatic force in electrospinning, the thin liquid film can form a chain of droplets sitting on the dual-wire. The complex morphology of the droplets can facilitate the surface jetting, and the intrinsic capillary force can further drive the emulsion to fill the gap between the two wires as a capillary pump.

Figure 14 illustrates the setup of a dual-wire emulsion electrospinning, which consists of a dual-wire spinneret (two closely parallel-positioned copper wires in this study), a rotary metal (aluminum) disk as fiber collector, and two high voltage direct-current (DC) power supplies carrying both the positive and negative voltage outputs, respectively. The use of the DC power supply with a negative voltage output as shown in Fig. 14 is to generate the potential of the fiber collector below the zero potential of all grounded surrounding pieces of equipment and lab utilities and thus to avoid the possible nanofibers flying off the fiber collector during manufacturing.

As shown in Fig. 14(a), the two closely positioned straight wires (metallic wires) function to manipulate and deliver a small quantity of liquid via capillary effect or mechanical motion through an emulsion reservoir.[80] Droplets sitting on a dual-wire spinneret can form either barrel-shaped droplets, which completely enwrap the wire segments, or droplet-bridges, which partially wet the wire segments, depending upon the wetting characteristic curves (W-curves) of the system.[80c] Superior to droplets sitting on a single wire, when the wire spacing of the dual-wire spinneret is very small, the gap between the two thin wires generates sufficient capillary force to pump the droplets to move along the wires in the form of droplet-bridge, i.e., wetting the wires or wicking. Recent experimental study [80b] has indicated that the wicking kinetics of droplet spreading on a dual-wire spinneret roughly obeyed the Lucas-Washburn law,[81] i.e., the meniscus displacement is proportional to the complete wicking time (i.e., the time interval from the start of droplet spreading to its disappearance) for a given fiber spacing. When applying a high DC voltage vertical to the plane of dual-wire spinneret, the electrocapillary force acting on the liquid-bridge can easily destabilize the liquid-bridge and form multiple

droplets as shown in Fig. 14(a); each droplet initiates one or multiple jets as shown in Fig. 14(b) due to the complex morphology of the droplets. When the two ends of the dual-wire spinneret are connected to an emulsion reservoir or a digitally controlled syringe pump, the electrocapillary force can drive the emulsion to the jetting zone [Fig. 14(b)]. The pumping process can also be realized via moving the dual-wire forth and back through the emulsion reservoir (mechanical translation). In addition, the use of dual-wire spinneret can significantly suppress the fast evaporation of the volatile solvent through reduction of the exposure of the emulsion to open air.

To validate the proposed dual-wire emulsion-electrospinning method, an emulsion was prepared via blending 10 wt. % polyacrylonitrile (PAN)/N,N-dimethyl formamide (DMF) and 10% isophorone diisocyanate (IPDI)/DMF solutions with the mass ratio 1:1 and tested on the basis of the proof-of-concept setup with varying parameters (See Experimental Section). Within the emulsion, the IPDI/DMF solution in the form of droplets dispersed inside the PAN/DMF solution as shown in Fig. 15. The resulting core-shell fibers were characterized using a diffractive optical microscope (IX 71 Olympus). Besides, Fig. 16 shows the snapshots of emulsion electrospinning of one emulsion droplet sitting on the dual-wire spinneret with increasing DC voltage between the wires and the fiber collector. As a result, continuous, scalable manufacturing of ultrathin core-shell fibers have been realized via dual-wire emulsion electrospinning.

Figure 17 shows the typical optical micrographs of the ultrathin core-shell IPDI/PAN fibers produced by the proposed dual-wire emulsion electrospinning setup, in which the diameter of the two identical copper wires is 0.28 mm and the wire spacing is 0.30 mm. It can be found from Fig. 17 that the core-shell fibers were well formed with uniform morphologies of the interior liquid IPDI core and exterior solid PAN shell. In this case, multiple measurements show that the average diameter of the IPDI core is 0.41 μm and the average exterior diameter of the PAN shell is 1.61μm. In addition, FT-IR was further used to validate the chemical composition of PAN/IPDI nanofibers. Figure 18 gives the comparison of FT-IR spectra between pure PAN nanofibers and PAN/IPDI core-shell fibers, which confirms the existence of IPDI in the core-shell fibers. In the spectra of PAN nanofibers, the characteristic absorption bands at 2920 cm-1, 2238 cm-1, 1662 cm-1 and 1449 cm-1 are assigned to v C - H stretching, v C ≡ N stretching, δC - H bond bending and δCH2 asymmetry, respectively.[82] In contrast, in the spectra of PAN/IPDI fibers, two

obvious peaks at ~2245 cm-1 and ~2920 cm-1 exist due to the isocyanate vN = C = O and v C - H stretching in IPDI, respectively.[83] Moreover, bands at 1627 cm-1 and 1563 cm-1 due to C = O vibration in the –NCO group indicate the existence of IPDI in the PAN/IPDI core-shell nanofibers.

Furthermore, to examine the effect of wire spacing on the geometries and morphology of the core-shell PAN/IPDI fibers, a dual-wire spinneret with zero spacing was further utilized while the rest process parameters were unaltered. Figure 19 shows the typical optical micrograph of the core-shell IPDI/PAN fibers. It can be observed that though the core-shell PAN/IPDI fibers had been well formed with smooth morphologies of the interior core and exterior shell, the diameter of the core-shell fibers had a large variation. Multiple measurements show that the average diameter of the IPDI core is 0.72 μm and the average diameter of the PAN shell is 1.95μm, which are much larger than those based on the dual-wire spinneret with the wire spacing of 0.30 mm.

Moreover, to take into account the effect of wire diameter on the diameter and morphology of the final core-shell PAN/IPDI fibers, a dual-wire spinneret with the wire diameter of 0.78 mm and wire spacing of 0.30 mm was further utilized and the rest process parameters were maintained the same. Figure 20 shows the typical optical micrograph of the core-shell PAN/IPDI fibers. From Fig. 20, it can be found that the core-shell PAN/IPDI fibers still carried well-formed morphologies of the interior core and exterior shell. However, the diameter of the core-shell fibers had a much larger variation than those in the above two cases. In this case, the average diameter of the IPDI core is 0.78 μm and the average diameter of the PAN shell is 2.02μm, slight larger than those based on the dual-wire spinneret with zero spacing. Therefore, the dual-wire spinneret is expected to offer a flexible manner to tailor the geometries of electrospun core-shell fibers.

In summary, a novel dual-wire emulsion electrospinning method is proposed and demonstrated for successful mass production of continuous core-shell nanofibers. The effects of the wire diameter and spacing on the nanofiber diameter have been examined. The proposed dual-wire needleless emulsion-emulsion method can be exploited for low-cost mass production of core-shell nanofibers for large scale applications of these novel ultrathin fibers.

a. Experimental

Polyacrylonitrile powder (PAN, Mw=150,000), liquid isophorone diisocyanate (IPDI), and N,N-dimethyl formamide (DMF) anhydrous 99.8% were purchased from Sigma-Aldrich (St. Louis, MO). To form the emulsion, two precursor solutions, i.e., a PAN/DMF solution with 10 wt. % PAN and an IPDI/DMF solution with 10 wt. % IPDI were first prepared via dissolving the PAN powder and liquid IPDI in DMF separately. The PAN/DMF and IPDI/DMF solutions had been continuously stirred on a hot-plate at 75 °C for 4 hours, and then blended together at the mass ratio 1:1. The resulting blend had been stirred on a hot-plate at 75 °C for another 4 hours and then stirred slowly at room temperature till the test.

The experimental setup is illustrated in Fig. 14 and characterized by a dual-wire spinneret of two parallel copper wires fixed on a metal fixture, a lab-made rotary aluminum disk (diameter: 25 cm and thickness: 2.5 mm), and two high voltage DC power supplies (Gamma High Voltage Research, Ormond Beach, FL) with the positive and negative voltage outputs, respectively. The rotary disk is placed parallel to the two-wire plane with a vertical distance ~30 cm and powered by a DC electrical motor with adjustable angular velocity. For comparative study, copper wires with two different diameters (0.28 mm and 0.78 mm) and two different values of spacing (0 mm and 0.30 mm) were selected for the dual-wire spinneret.

The dual-wire emulsion-electrospinning test was performed at room temperature. Prior to the test, the two wires of the spinneret were cleaned with acetone to maintain largely constant surface energy of the wires. Given a set of parameters (i.e., wire diameter and spacing) of the dual-wire spinneret, the emulsion was first delivered to the spinneret manually for form multiple droplet-bridges as illustrated in Fig. 14. Once applying the DC voltage +25 kV to the spinneret and -20 kV to the fiber collector, multiple jets initiated from each droplet bridge as illustrated in Fig. 15. The obtained ultrathin core-shell PAN/IPDI fibers were characterized using an optical microscope (IX 71 Olympus with the objective magnification 40).

The present invention is not to be limited to the particular embodiments described herein. In particular, the present invention contemplates numerous variations in the type of ways in which embodiments of the invention may be applied to [Insert high-level or more detailed description of the invention]. The foregoing description has been presented for

purposes of illustration and description. It is not intended to be an exhaustive list or limit any of the disclosure to the precise forms disclosed. It is contemplated that other alternatives or exemplary aspects that are considered included in the disclosure. The description is merely examples of embodiments, processes or methods of the invention. It is understood that any other modifications, substitutions, and/or additions may be made, which are within the intended spirit and scope of the disclosure. For the foregoing, it can be seen that the disclosure accomplishes at least all of the intended objectives.

The previous detailed description is of a small number of embodiments for implementing the invention and is not intended to be limiting in scope. The following claims set forth a number of the embodiments of the invention disclosed with greater particularity.

REFERENCES

1. S. W. Tsai, "Three decades of composites activities at US Air Force Materials Laboratory," Compos. Sci. Technol. 2005; 65: 2295– 2299.

2. T. W. Chou, Microstructural Design of Fiber Composites, Cambridge: Cambridge University Press, 1992.

3. R. M. Jones, Mechanics of Composite Materials (2nd Ed.), Philadelphia: Taylor and Francis, 1999.

4. R. A. Lane, "High performance fibers for personnel and vehicle armor systems-Putting to a stop to current and future threats," AMPTIC 2005; 9: 3-9.

5. D. Tenney and R. B. Pipes, "Advanced composites development for aerospace applications," The 7th Japan Int. SAMPE Sym. Exhibition, Tokyo, Japan, 2001-11-13.

6. R.S. Trask, G.J. Williams, and I.P. Bond, "Self-healing polymer composites: mimicking nature to enhance performance," Bioinsp. Biomim. 2007; 2: 1-9.

7. S. R. White, N.R. Sottos, J. Moore, P. Geubelle, M. Kessler, E. Brown, S. Suresh, and S. Viswanathan, "Autonomic healing of polymer composites," Nature 2001, 409: 794-797.

8. R. P. Wool, "A material fix," Nature 2001, 409: 794-797.

9. N. Sottos, S. White, and I. Bond, "Introduction: Self-healing polymer and composites," J. R. Soc. Interface 2007, 4: 347-348.

10. S. van der Zwaag, Self-Healing Materials-An Alternative Approach to 20 Centuries of Materials Science, Springer: Heidelberg, 2007.

11. D. G. Schulin and H. Möhwald, "Self-repairing coating containing active nanoreservoirs," Small 2007, 3: 926-943.

12. D. Y. Wu, S. Meure, and D. Solomon, "Self-healing polymeric materials: A review of recent developments," Prog. Polym. Sci. 2008, 33: 479-522.

13. B. J. Blaiszik, S. L. B. Kramer, S. C. Olugebefola, J. S. Moore, N. R. Sottos, and S. R. White, "Self-healing polymers and composites," Annu. Rev. Mater. Res. 2010, 40: 179-211.

14. E. B. Murphy and F. Wudl, "The world of smart healable materials," Prog. Polym. Sci. 2010, 35: 223-251.

15. C. W. Bielawski and R. H. Grubbs, "Living ring-opening metathesis polymerization," Prog. Polym. Sci. 2007; 32: 1-29.

16. M. R. Kessler, N. R. Sottos, and S. R. White, "Self-healing structural composite materials," Composites A 2003, 34: 743-753.

17. E. N. Brown, S. R. White, and N. R. Sottos, "Retardation and repair of fatigue cracks in a microcapsule toughened epoxy composite-Part I: Manual infiltration," Compos. Sci. Technol. 2005; 65: 2466-2473.

18. E. N. Brown, S. R. White, and N. R. Sottos, "Retardation and repair of fatigue cracks in a microcapsule toughened epoxy composite-Part II: in situ self-healing," Compos. Sci. Technol. 2005; 65: 2474-2480.

19. J. D. Rule, N. R. Sottos, and S. R. White, "Effect of microcapsule size on the performance of self-healing polymers," Polymer 2007, 48: 3520-3529.

20. A. S. Jones, J. D. Rule, J. S. Moore, N. Sottos, S. White, "Life extension of self-healing polymers with rapidly growing fatigue cracks," J. R. Soc. Interface 2007, 4:395-403.

21. T. Yin, M. Z. Rong, M. Q. Zhang, and G. C. Yang, "Self-healing epoxy composites-Preparation and effect of the healant consisting of microencapsulated epoxy and latent curing agent," Compos. Sci. Technol. 2007, 67: 201-212.

22. B. J. Blaiszik, N. R. Sottos, and S. R. White, "Nanocapsules for self-healing materials," Compos. Sci. Technol. 2008, 68: 978-986.

23. A. J. Patel, N. R. Sottos, E. D. Wetzel, and S. R. White, "Autonomic healing of low-velocity impact damage in fiber-reinforced composites," Composites A 2010, 41: 360-368.

24. S. H. Cho, S. R. White, and P. V. Braun, "Self-healing polymer coatings," Adv. Mater. 2008; 20: 1-5.

25. M. X. Huang and J. L. Yang, "Facile microencapsulation of HDI for self-healing anticorrosion coatings," J. Mater. Chem. 2011, 21: 11123.

26. S. M. Bleay, C. B. Loader, V. J. Hawyes, L. Humberstone, and P. T. Curtis, "A smart repair system for polymer matrix composites," Composites A 2001, 32: 1767-1776.

27. J. W. C. Pang and I. P. Bond, "'Bleeding composites'-damage detection and self-repair using a biomimetic approach," Composites A 2005, 36: 183-188.

28. J. W. C. Pang and I. P. Bond, "A hollow fibre reinforced polymer composite encompassing self-healing and enhanced damage visibility," Compos. Sci. Technol. 2005, 65: 1791-1799.

29. S. A. Hayes, F.R. Jones, K. Marshiya, W. Zhang, "A self-healing thermosetting composite material," Composites A 2007, 38: 1116- 1120.

30. R. S. Trask, G. J. Williams, and I. P. Bond, "Bioinspired self-healing of advanced composite structures using hollow glass fibres," J. R. Soc. Interface 2007, 4: 363-371.

31. C. J. Hansen, W. Wu, K. S. Toohey, N. R. Sottos, S. R. White, and J. A. Lewis, "Self-healing materials with interpenetrating microvascular networks," Adv. Mater. 2009, 21: 4143-4147.

32. J. H. Park, P. V. Braun, "Coaxial electrospinning of self-healing coatings," Adv. Mater. 2010, 22: 496-499.

33. S. C. Olugebefola, A. M. Aragón, C. J. Hansen, A. R. Hamilton, B. D. Kozola, W. Wu, P. H. Geubelle, J. A. Lewis, N. R. Sottos, and S. R. White, "Polymer microvascular network composites," J. Compos. Mater. 2010, 44: 2587-2603.

34. K. Dransfield, C. Baillie, and Y. W. Mai, "Improving the delamination resistance of CFRP by stitching-A review," Compos. Sci. Technol. 1994, 50: 305-317.

35. A.C. Garg and Y.W. Mai, "Failure mechanisms in toughened epoxy resins-A review," Compos. Sci. Technol. 1988, 31: 179-223.

36. I. M. Low and Y. M. Mai, "Fracture properties and failure mechanism of pure and toughened epoxy resins," in Handbook of Ceramics and Composites (edited by N. P. Cheremisinoff), 1990, 2: 105-150.

37. J.-K. Kim and Y.-W. Mai, "High strength, high fracture toughness fiber composites with interface control-A review," Compos. Sci. Technol. 1991, 41: 333-378.

38. L. A. Carlsson and A. Aksoy, "Analysis of interleaved end-notched flexure specimen for measuring mode II fracture toughness," Int. J. Fracture 1999, 52: 67-77.

39. R. B. Pipes and N. J. Pagano, "Interlaminar stresses in composite laminates under uniform axial extension," J. Compos. Mater.
1970; 4: 538-548.

40. N. J. Pagano, "On the calculation of interlaminar normal stress in composite laminate," J. Compos. Mater. 1974, 8: 65-81.

41. Y. Dzenis, "Structural nanocomposites," Science, 2008, 319: 419-420.

42. Y. A. Dzenis and D. H. Reneker, "Delamination resistant composites prepared by small diameter fiber reinforcement at ply interfaces," US Patent 6265333, 2001.

43. J. Doshi and D. H. Reneker, "Electrospinning process and applications of electrospun fibers," J. Electrostatics, 1995, 35: 151-160.

44. D. H. Reneker and I. Chun, "Nanometre diameter fibres of polymer, produced by electrospinning," Nanotechnology, 1996, 7: 216- 223.

45. Y. Dzenis, "Spinning continuous nanofibers for nanotechnology," Science, 2004, 304, 1917-1919.

46. D. H. Reneker, A. L. Yarin, E. Zussman, and H. Xu, "Electrospinning of nanofibers from polymer solutions and melts," Adv. Appl.
Mech. 2007, 41, 43-195.

47. D. H. Reneker and A. L. Yarin, "Electrospinning jets and polymer nanofibers," Polymer, 2008, 49, 2387-2425.

48. A. Greiner and J. H. Wendorff, "A fascinating method of preparation of ultrathin fibers" Angewandte Chemie- International Eddition, 2007, 46: 5670-5703.

49. X. F. Wu, Fracture of Advanced Composites with Nanostructured Interfaces: Fabrication, Characterization and Modeling.VDM Verlag, Germany, 2009.

50. Q. Chen, L. F. Zhang, M. K.Yoon, X. F. Wu, R. H. Arefin, and H. Fong, "Epoxy composites reinforced and/or toughened with electrospun SiO2 nanofibers," J. Appl. Polym. Sci. 2012, 124: 444-451.

51. Q. Chen, L. F. Zhang, A. Rahman, Z. P. Zhou, X. F. Wu, and H. Fong, "Hybrid multi-scale epoxy composite made of conventional carbon fiber fabrics with interlaminar regions containing electrospun carbon nanofiber mats," Composites A 2011, 42: 2036-2042.

52. Q. Chen, L. F. Zhang, Y. Zhao, X. F. Wu, and H. Fong, "Hybrid multi-scale composites developed from glass microfiber fabrics and nano-epoxy resins containing electrospun glass nanofibers," Composites B, 2012: 43, 309-316.

53. Z. Sun, E. Zussman, A. L. Yarin, J. H. Wendorff, and A. Greiner, "Compound core-shell polymer nanofibers by co- electrospinning," Adv. Mat. 2003, 15: 1929.

54. A. L. Yarin, "Coaxial electrospinning and emulsion electrospinning of core-shell fibers,"Polym. Adv. Technol. 2011, 22: 310-317.

55. S. Sinha-Ray, D. D. Pelot, Z. P. Zhou, A. Rahman, X. F. Wu, and A. L. Yarin, "Encapsulation of self-healing materials by coelectrospinning, emulsion, electrospinning, and solution blowing and intercalation," J. Mater. Chem. 2012, 22: 9138-9146.

56. A. Rahman, Fabrication and Mechanical Characterization of Novel Hybrid Carbon-Fiber/Epoxy Composites Reinforced with Toughening/Self-Repairing Nanofibers at Interfaces (M.S. Thesis), North Dakota State University, ND, USA, 2011.

57. X. F. Wu and Y. A. Dzenis, "Experimental determination of probabilistic edge-delamination strength of a graphite-fiber/epoxy composite," Compos. Struct. 2005, 70: 100-108.

58. Z. C. Sun, E. Zussman, A. L. Yarin, J. H. Wendorff, and A. Greiner, "Compound core-shell polymer nanofibers by co- electrospinning," Advanced Materials 15, 1929-1932 (2003).

59. D. Li, A. Babel, S. A. Jenekle, and Y. N. Xia, "Nanofibers of conjugated polymer prepared by electrospinning with two-capillary spinneret," Advanced Materials 16, 2062-2066 (2004).

60. J. T. McCann, D. Li, and Y. N. Xia, "Electrospinning of nanofibers with core-sheath, hollow, or porous structures," Journal of Materials Chemistry 15, 735-738 (2005).

61. A. L. Yarin, "Coaxial electrospinning and emulsion electrospinning of core-shell fibers," Polymers Advanced Technologies 22, 310-317 (2011).

62. S. Sinha-Ray, D. D. Pelot, Z. P. Zhou, A. Rahman, X.- F. Wu, and A. L. Yarin, "Encapsulation of self-healing materials by coelectrospinning, solution blowing and intercalation," Journal of Materials Chemistry 22, 9138-9146 (2012).

63. A. K. Moghe and B. S. Gupta, "Co-axial electrospinning for nanofiber structures: Preparation and applications," Polymer Reviews

48, 353-377 (2008).

64. A. V. Bazilevsky, A. L. Yarin, and C. M. Megaridis, "Co-electrospinning of core-shell fibers using a single-nozzle technique,"
Langmuir 23, 2311-2314 (2007).

65. X. F. Wu, A. Bedarkar, and K. A. Vaynberg, "Droplets wetting on filament rails: Surface energy and morphology transition," Journal of Colloids and Interface Science 341, 326-332 (2011).

66. A. Bedarkar, X. F. Wu, and A. Vaynberg, "Wetting of liquid droplets on two parallel filaments," Applied Surface Science 256, 7260-7264 (2010).

67. K. Keis, K. G. Kornev, A. V. Neimark, and Y. K. Kamath, "Towards fiber-based micro-and nano fluidics," in "Nanoengineered Nanofibrous Materials," S. Guceri, Y. G. Gogoti, and V. Kuznetsov (eds.), NATO Science Series II: Mathematics, Physics and Chemistry 169, 175-182 (2004).

68. H. M. Princen, "Capillary phenomena in assemblies of parallel cylinders III. Liquid column between horizontal parallel cylinders," Journal of Colloid and Interface Science 34, 171-184 (1970).

69. a) D. H. Reneker, I. Chun, Nanotechnology 1996, 77, 216. b) J. Doshi, D. H. Reneker, J. Electrostatics 1995, 35 151. c) Z. M. Huang, Y. Z. Zhang, M. Kotaki, S. Ramakrishna, Compos. Sci. Tech. 2003, 63, 2223. d) Y. Dzenis, Science 2004, 304, 1917. e) D. Li, Y. N. Xia, Adv. Mater. 2004, 16, 1151. f) D. H. Reneker, A. L. Yarin, E. Zussman, H. Xu, Adv. Appl. Mech. 2007, 41, 43. g) A. Greiner, J. H. Wendorff, Angew. Chem. Int. Ed. 2007, 46, 5670. h) R. Ramaseshan, S. Sundarragan, R. Jose, S. Ramakrishna, J. Appl. Phys. 2007, 102, 111101. i) D. H. Reneker, A. L. Yarin, Polymer 2008, 49, 2387.

70. a) P. Gibson, H. Schreuder-Gibson, D. Rivin, Colloids Surfaces A –Physicochem. Eng. Asp. 2001, 187, 469. b) D. Smith, D. H. Reneker, W. Kataphinan, A. Dabney, US Patent 2001, 6821479. c) D. Smith, D. H. Reneker, US Patent 2004, 6753454.

71. a) R. Gopal, S. Kaur, Z. W. Ma, C. Chan, S. Ramakrishna, T. Matsuura, J. Membrane Sci 2006, 281, 581. b) B. Maze, H. V. Tafreshi, Q. Wang, B. Pourdeyhimi, Aerosol Sci. 2007, 38, 550. c) R. S. Barhate, S. Ramakrishna, J. Membrane Sci. 2007, 296, 1.

72. a) Y. Dzenis, Science 2008, 319, 419. b) F. Chen, X. W. Peng, T. T. Li, S. L. Chen, X. F. Wu, D. H. Reneker, H. Q. Hou, J. Phys. D: Appl. Phys. 2008, 41, 025308. c) C. Y. Cheng, J. Chen, F. Chen, X. F. Wu, D. H. Reneker, H. Q. Hou, J. Appl. Polym. Sci. 2010, 116, 1581. d) Q. Chen, L. F. Zhang, A. Rahman, Z. P. Zhou, X. F. Wu, H. Fong, Composites A: Manufact. Appl. Sci. 2011, 42, 2036. e) Q. Chen, L. F. Zhang, Y. Zhao, X. F. Wu, H. Fong, Composites B: Engineering 2012, 43, 309. f) Q. Chen, L. F. Zhang, M. K. Yoon, X. F. Wu, R. H. Arefin, H. Fong, J. Appl. Polym. Sci. 2012, 124, 444.

73. a) W. J. Li, C. T. Laurencin, E. J. Caterson, R. S. Tuan, F. K. Ko, J. Biomed. Mater. Res. 2002, 60, 613. b) J. A. Matthews, G. E. Wnek, D. G. Simpson, G. L. Bowlin, Biomacromolecules 2002, 3, 232. c) C. Burger, B. S. Hsiao, B. Chu, Ann. Rev. Mater. Res. 2006, 36, 333. d) Q. P. Pham, U. Sharma, A. G. Mikos, Tissue Eng. 2006, 12, 1197. e) C. P. Barnes, S. A. Sell, E. D. Boland, D. G. Simpson, G. L. Bowlin, Adv. Drug Delivery Rev. 2007, 59, 1413. f) J. Xie, X. Li, Y. Xia, Nature Mat. 2008, 29, 1775.

74. a) E. R. Kenawy, G. L. Bowlin, K. Mansfield, J. Layman, D. G. Simpson, E. H. Sanders, G. E. Wnek, J. Contr. Release 2002, 81, 57. b) S. Y. Chew, Y. Wen, Y. Dzenis, K. W. Leong, Current Pharm. Design 2006, 12, 4751. c) D. H. Liang, B. S. Hsiao, B. Chu, Adv. Drug Delivery Rev. 2007, 59, 1392.

75. a) C. Kim, K. S. Yang, Appl. Phys. Lett. 2003, 83, 1216. b) C. Kim, B. T. N. Ngoc, K. S. Yang, M. Kojima, Y. A. Kim, Y. J. Kim, M. Endo, S. C. Yang, Adv. Mater. 2007, 19, 2341. c) L. W. Ji, X. W. Zhang, Carbon 2009, 47, 3219. d) D. L. Schulz, J. Hoey, J. Smith, A. Elangovan, X. Wu, I. Akhatov, S. Payne, J. Moore, P. Boudjouk, L. Pederson, J. Xiao, J. Zhang, Electrochem. Solid State Lett. 2010, 13, A143. e) X. W. Zhang, L. W. Ji, O. Toprakci, Y. Z. Liang, M. Alcoutlabi, Polym. Rev. 2011, 51, 239. f) Z. P. Zhou, X. F. Wu, H. Fong, Appl. Phys. Lett. 2012, 100, 023115.

76. a) Z. C. Sun, E. Zussman, A. L. Yarin, J. H. Wendorff, A. Greiner, Adv. Mater. 2003, 15, 1929. b) D. Li, A. Babel, S. A. Jenekle, Y. N. Xia, Adv. Mater. 2004, 16, 2062. c) J. T. McCann, D. Li, Y. N. Xia, J. Mater. Chem. 2005, 15, 735. A. K. Moghe, B. S. Gupta, Polym. Rev. 2008, 48, 353.

77. S. Sinha-Ray, D. D. Pelot, Z. P. Zhou, A. Rahman, X. F. Wu, A. L. Yarin, J. Mater. Chem. 2012, 22, 9138.

78. a) A. V. Bazilevsky, A. L. Yarin, C. M. Megaridis, Langmuir 2007, 23, 2311. b) X. L. Xu, X. L. Zhuang, X. S. Chen, X. R. Wang, L. X. Yang, X. B. Jing, Macromol. Rapid Commun. 2006, 27, 1637. c) A. L. Yarin, Polym. Adv. Tech. 2011, 22, 310.

79. a) A. L. Yarin, E. Zussman, Polymer 2004, 45, 2977. b) A. Theron, A. L. Yarin, E. Zussman, E. Kroll, Polymer 2005, 46, 2889. c) X. F. Wu, Y. A. Dzenis, J. Phys. D 2005, 38, 2848. d) D. Lukas, A. Sarkar, P. Pokorny, J. Appl. Phys. 2008, 103, 084309. e) T. Miloh, B. Spivak, A. L. Yarin, J. Appl. Phys. 2009, 106, 114910. f) D. Lukas, A. Sarkar, L. Martinova, K. Vodsedalkova, D. Lubasova, J. Chaloupek, P. Pokorny, P. Mikes, J. Chvojka, M. Komarek, Textile Prog. 2009, 41, 59.

80. a) H. M. Princen, J. Colloid Interface Sci. 1970, 34, 171. b) S. Guceri, Y. G. Gogoti, and V. Kuznetsov (eds.), NATO Science Series II: Mathematics, Physics and Chemistry 2004, 169, 175. c) X. F. Wu, A. Bedarkar, K. A. Vaynberg, J. Colloids Interface Sci. 2010, 341, 326. d) A. Bedarkar, X. F. Wu, A. Vaynberg, Appl. Surface Sci. 2010, 256, 7260.

81. a) R. Lucas, Kollid Z. 1918, 23, 15. b) E.W. Washburn, Phys. Rev. 1921, 17, 273.

82. M. Moreno, M. A. S Ana, G. Gonzalez, E. Benavente, Electrochim. Acta 2010, 55, 1323.

83. S. J. Zhou, C. Y. Ma, Y. Y. Meng, H. F. Su, Z. Zhu, S. L. Deng, S. Y. Xie, Nanotechnology 2012, 23. 055708.

What is claimed is:

1. A self-repairing composite, comprising:
   a. one or more interfacial regions;
   b. at least one fiber having a hollow core;
   c. one or more self-repairing agents housed in the hollow core; and
   d. the at least one hollow core fiber incorporated at the one or more interfacial regions for repairing the composite.

2. The self-repairing composite of claim 1 wherein the hollow-core fiber comprises an interlayer of the composite.

3. The self-repairing composite of claim 1 wherein the one or more self-repairing agents include on of:
   a. a monomer;
   b. a polymer.

4. The self-repairing composite of claim 1 further comprising:
at least one film comprising the hollow-core fiber at the one or more interfacial regions between ply surfaces of the composite.

5. The self-repairing composite of claim1 wherein self-repair of the composite by the self-repairing agent comprises ring-open polymerization.

6. The self-repairing composite of claim 1 further comprising:
a fiber volume fraction of the less than 1%.

7. The self-repairing composite of claim 1 further comprising:
at least one film comprising the hollow-core fiber at the one or more interfacial regions between fiber fabric surfaces of the composite.

8. The self-repairing composite of claim 1 wherein the fiber has an outer diameter generally between 200nm and a few micrometers.

9. A method for manufacturing self-repairing composites, comprising:
providing a fiber collector and a pair of closely spaced conductive wires comprising a dual-wire spinneret;
delivering a two-compound emulsion along the dual-wire spinneret;
applying a voltage between the dual-wire spinneret and the film collector;
ejecting one or more emulsion jets from the dual-wire spinneret; and
stretch-forming the second solution under electrostatic force into a core of the first solution.

10. The method of claim 9 further comprising:
depositing the one or more jets on the fiber collector, wherein the deposition comprises a core-shell fiber mat.

11. The method of claim 9 wherein the two-compound emulsion comprises two or more immiscible polymers.

12. The method of claim 9 wherein each emulsion jet comprises droplets of a first polymer solution enwrapping droplets of a second polymer solution.

13. The method of claim 9 further comprising:
controlling the one or more emulsion jets at least in part by adjusting thermodynamic equilibrium of the two-compound emulsion

14. The method of claim 9 further comprising:
evaporating a solvent in the one or more emulsion jets before deposition on the fiber collector.

15. The method of claim 9 wherein the first solution comprises isophorone diisocyanate (IPDI).

16. The method of claim 9 wherein the second solution comprises polyacrylonitrile (PAN).

17. A self-repairing fiber, comprising:

a fiber shell having terminal ends, the fiber shell formed from a two or more compound solution;

a fiber core enwrapped by the fiber shell at least between the terminal ends, the fiber core formed from the two or more compound solution; and

wherein the fiber core comprises one or more self-repairing agents.

18. The self-repairing fiber of claim 17 wherein the fiber shell has an outer diameter generally between 200nm – 2μm.

19. The self-repairing fiber of claim 17 wherein the one or more self-repairing agents comprise a liquid monomer or a liquid polymer.

20. The self-repairing fiber of claim 17 wherein the fiber shell comprises a hollow core with the one or more self-repairing agents operable by ring-open polymerization.

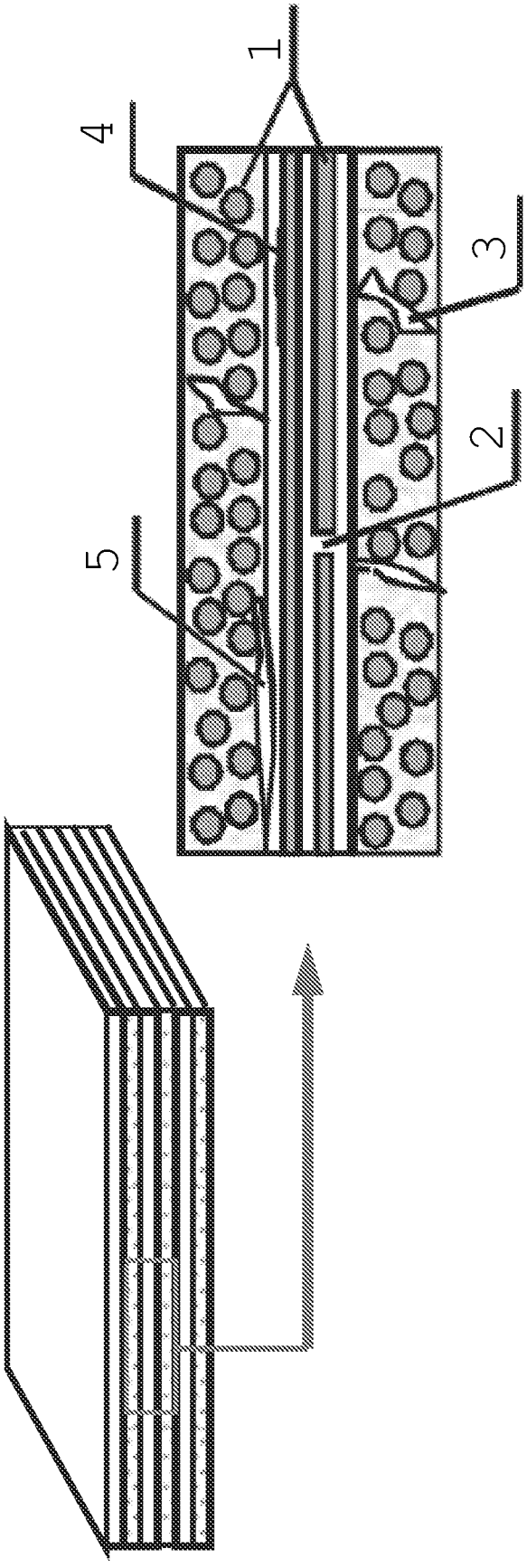

FIG. 1

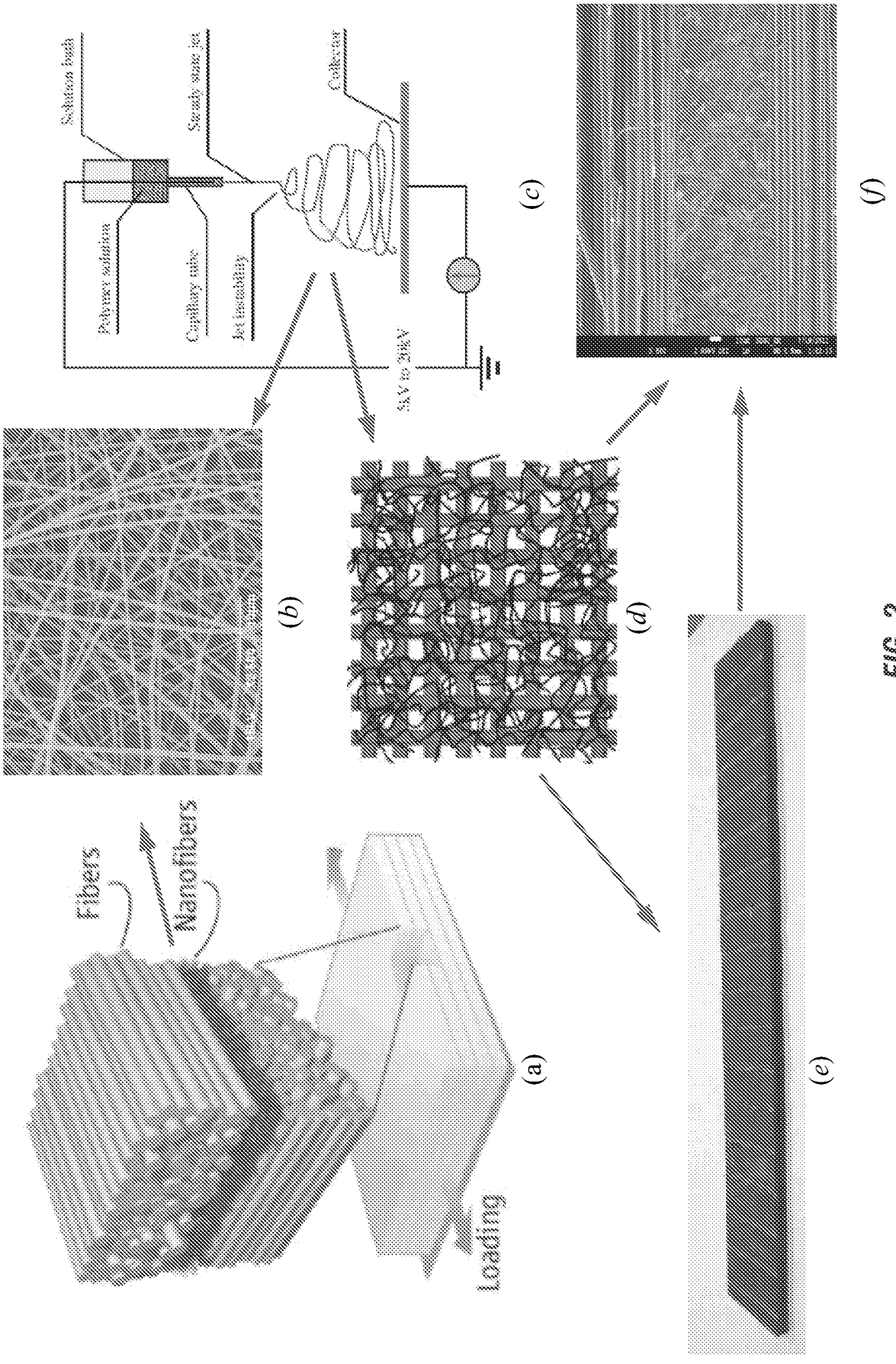
Fibers
Nanofibers
Loading
(a)
(b)
(c)
(d)
(e)
(f)
Solution bath
Steady state jet
Collector
Polymer solution
Capillary tube
Jet instability
5kV to 20kV

FIG. 2

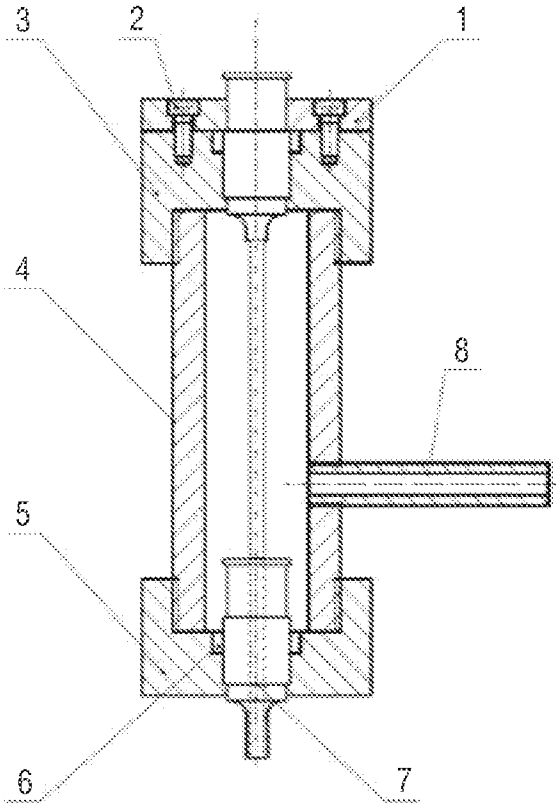

(a)

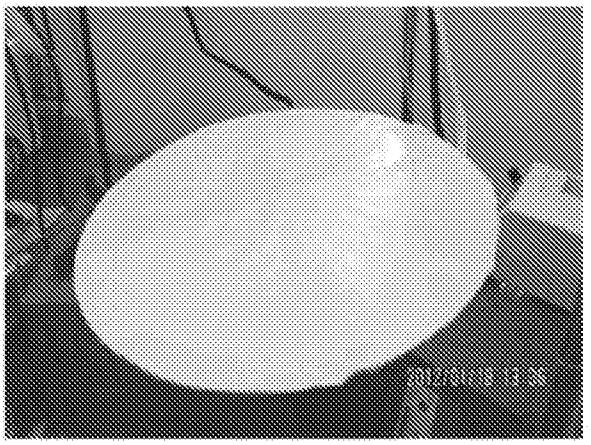

(b)

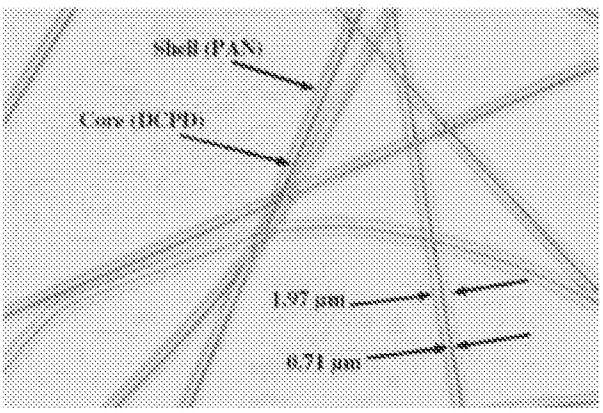

(c)

FIG. 3

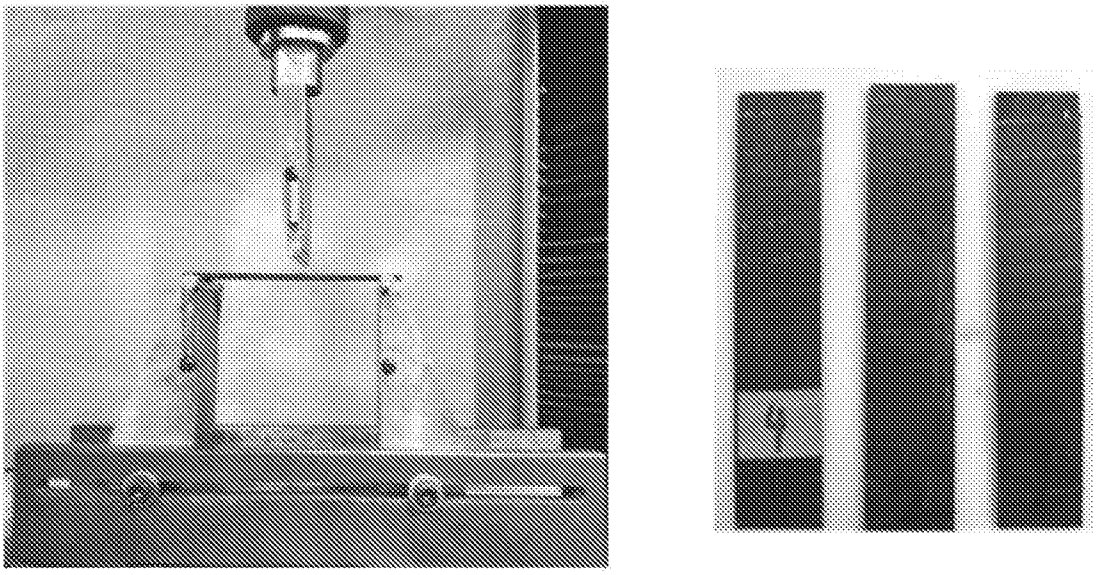

(a) (b)

FIG. 4

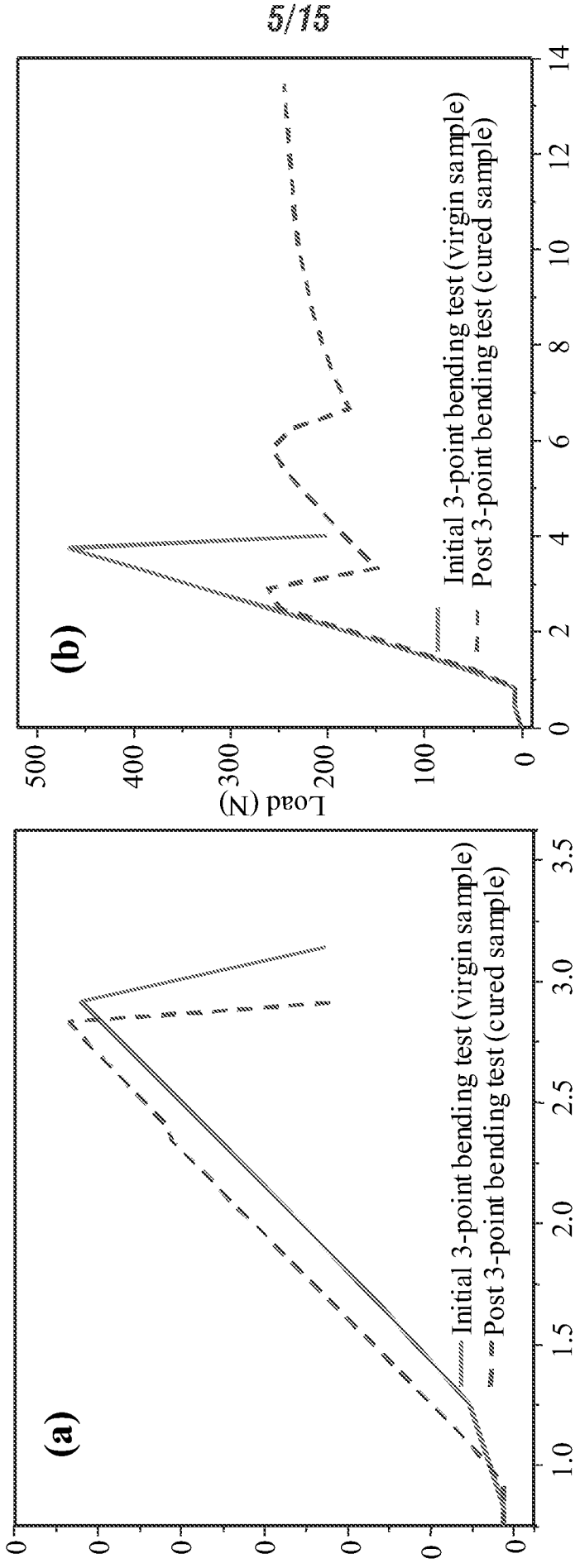
(a)
Initial 3-point bending test (virgin sample)
Post 3-point bending test (cured sample)
Deflection (mm)
1.0
1.5
2.0
2.5
3.0
3.5
(b)
Load (N)
Initial 3-point bending test (virgin sample)
Post 3-point bending test (cured sample)
Deflection (mm)
0
100
200
300
400
500
0
2
4
6
8
10
12
14

FIG. 5

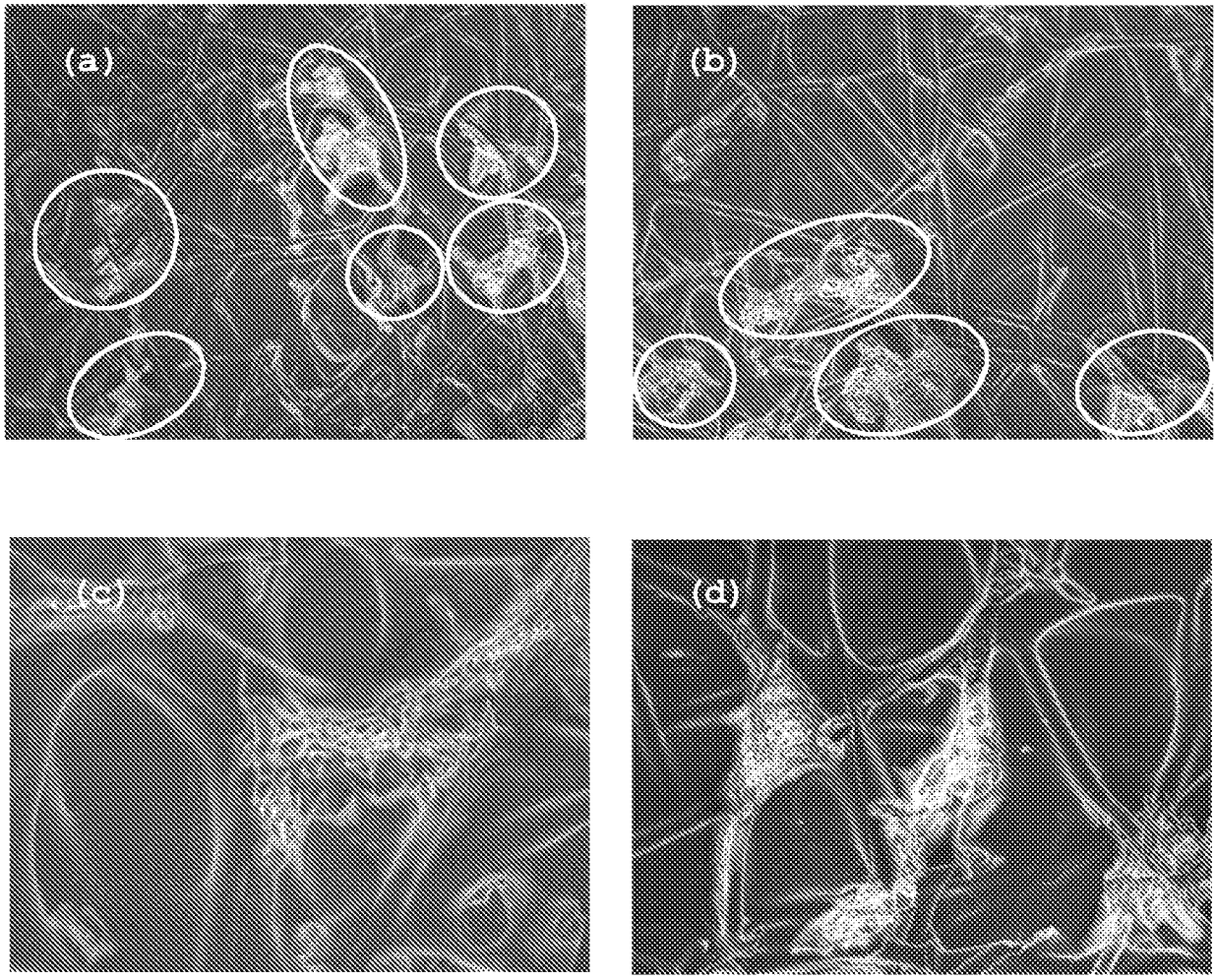

FIG. 6

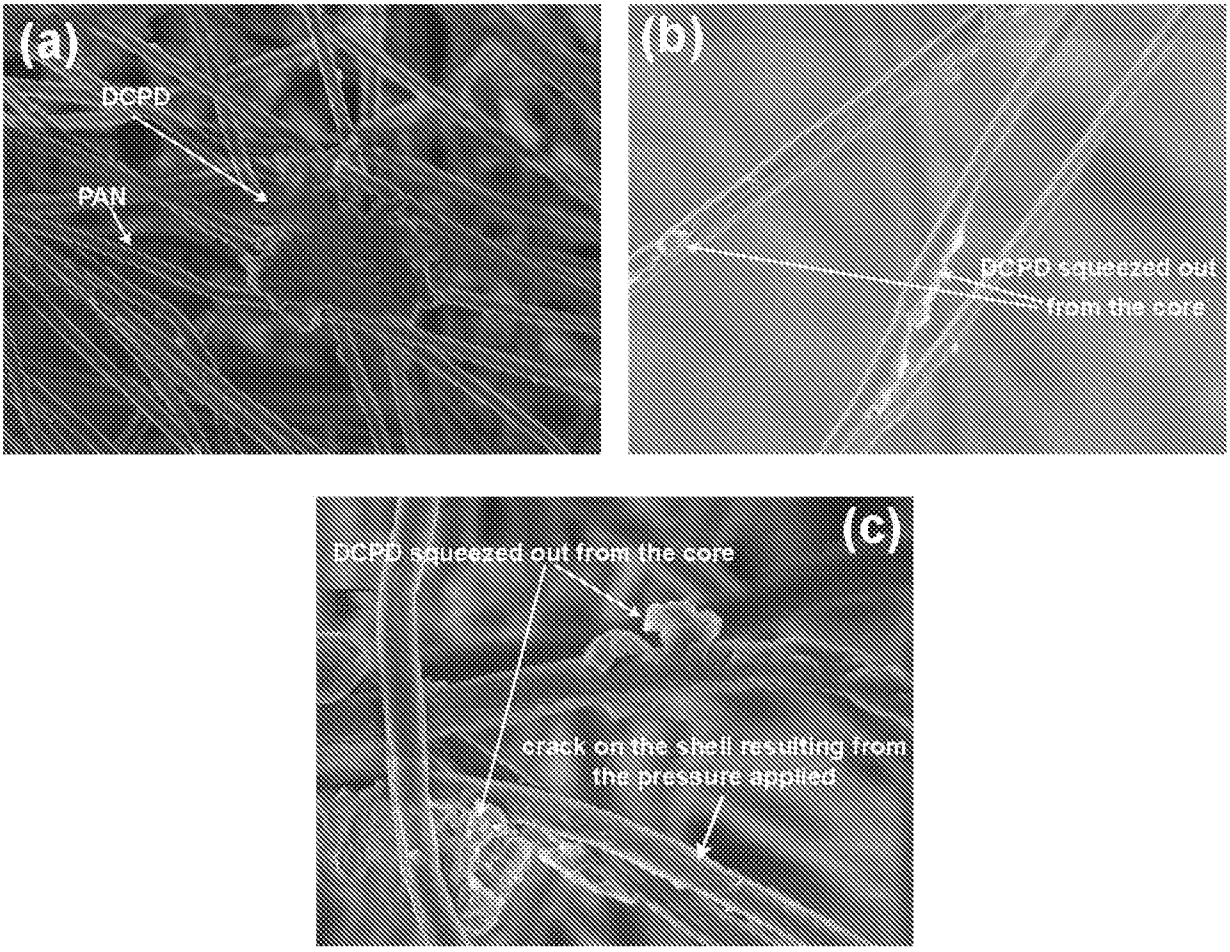
(a)
DCPD
PAN
(b)
DCPD squeezed out from the core
DCPD squeezed out from the core
(c)
crack on the shell resulting from the pressure applied

FIG. 7

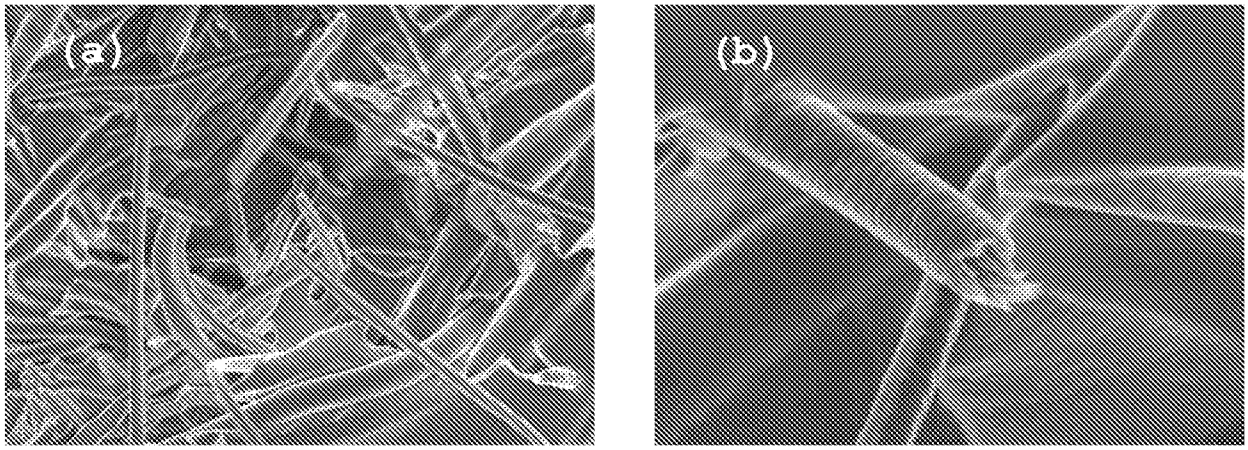

FIG. 8

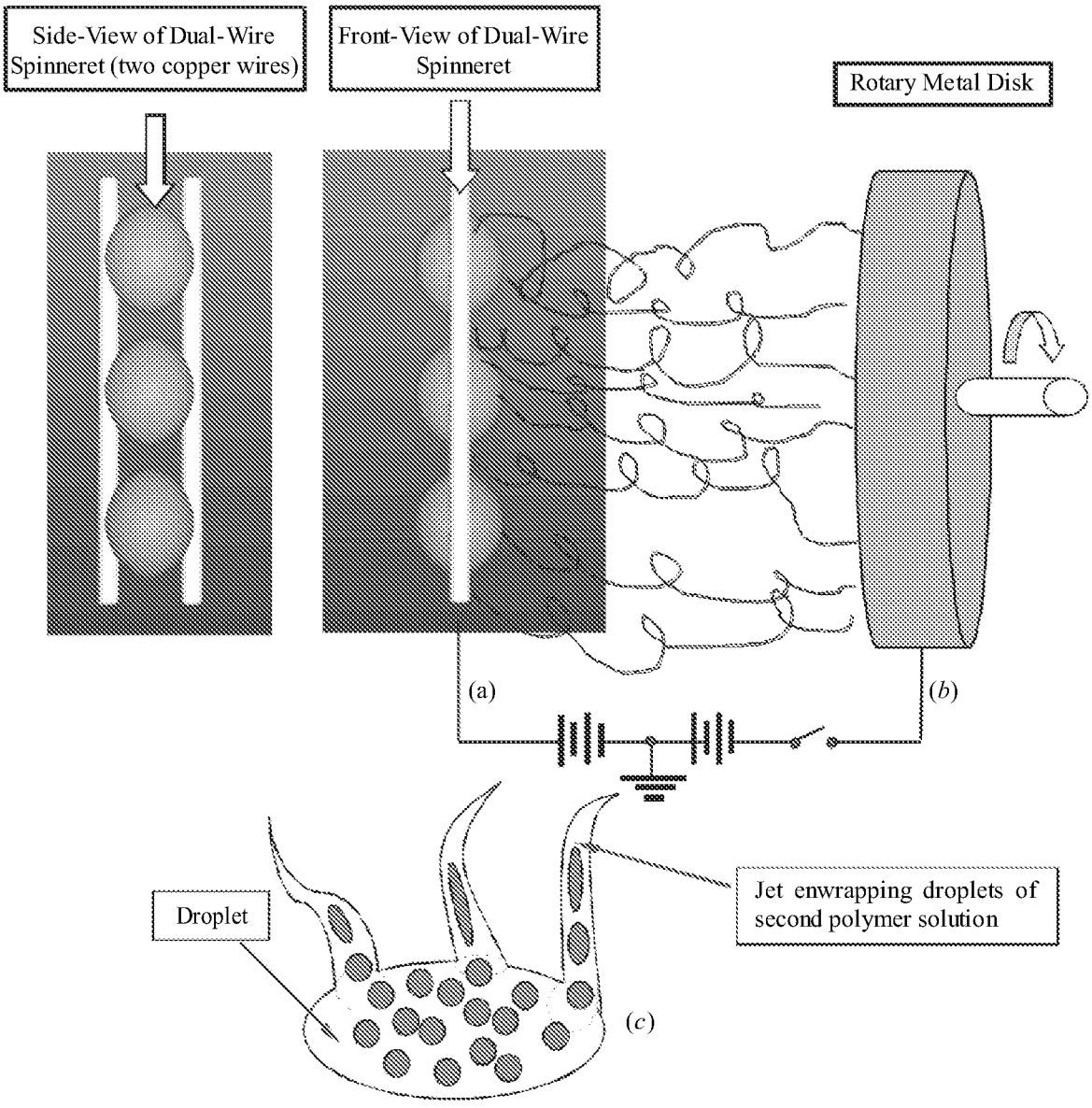
Side-View of Dual-Wire Spinneret (two copper wires)
Front-View of Dual-Wire Spinneret
Rotary Metal Disk
(a)
(b)
Droplet
Jet enwrapping droplets of second polymer solution
(c)

FIG. 9

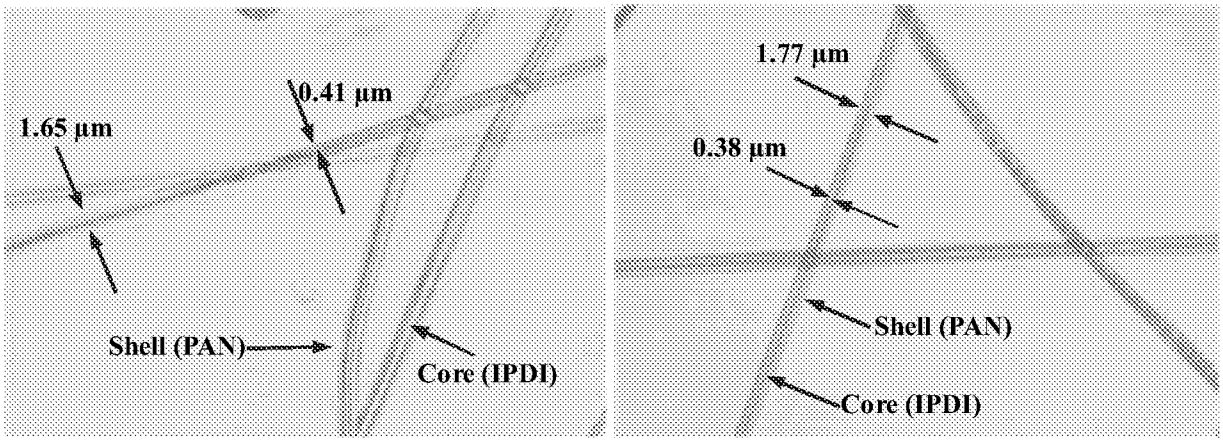
1.65 µm
0.41 µm
Shell (PAN)
Core (IPDI)
1.77 µm
0.38 µm
Shell (PAN)
Core (IPDI)

FIG. 10

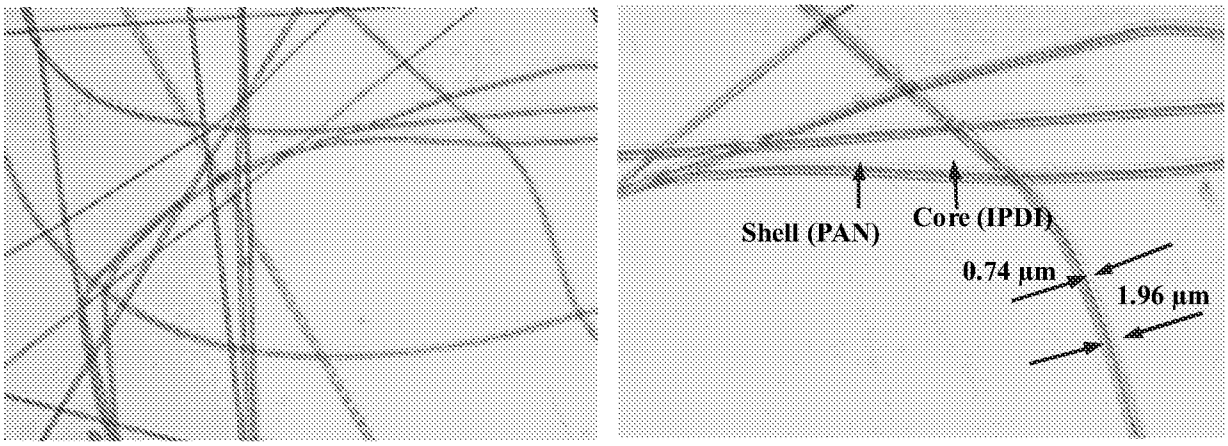
Shell (PAN)
Core (IPDI)
0.74 µm
1.96 µm

FIG. 11

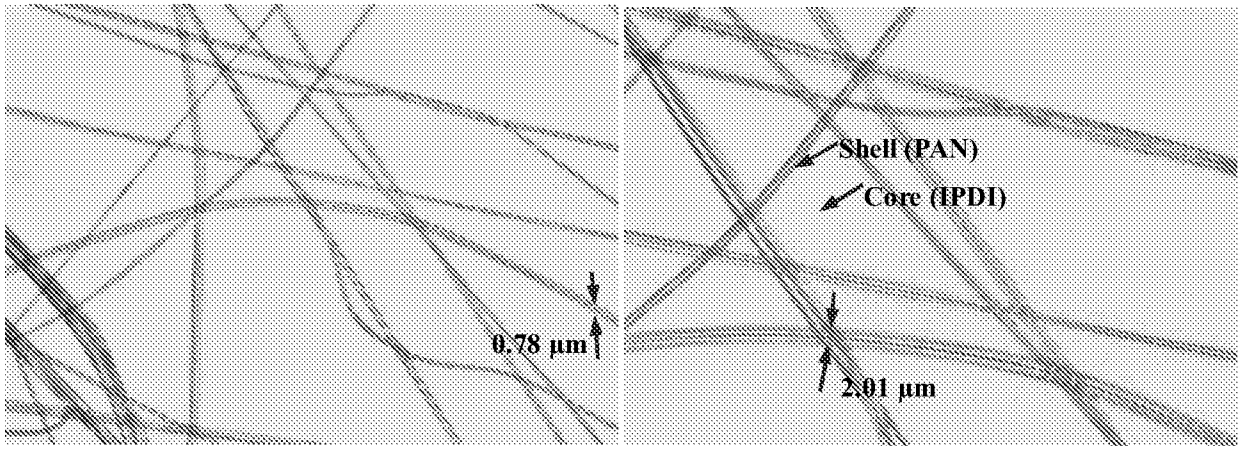

FIG. 12

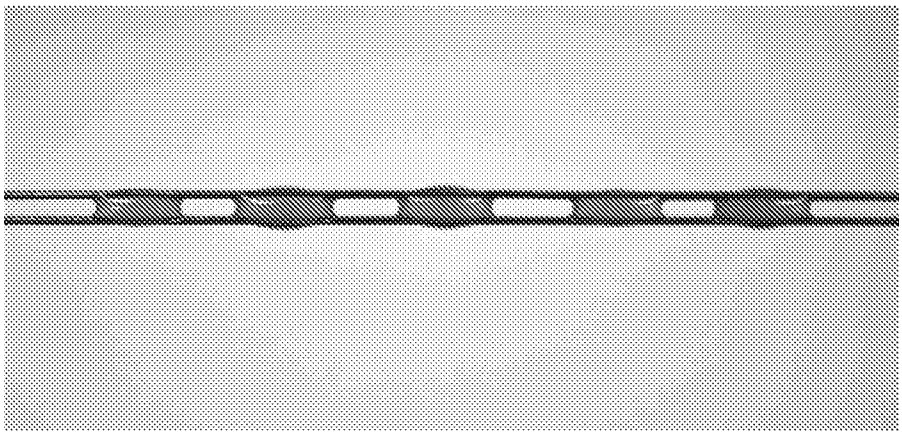

FIG. 13

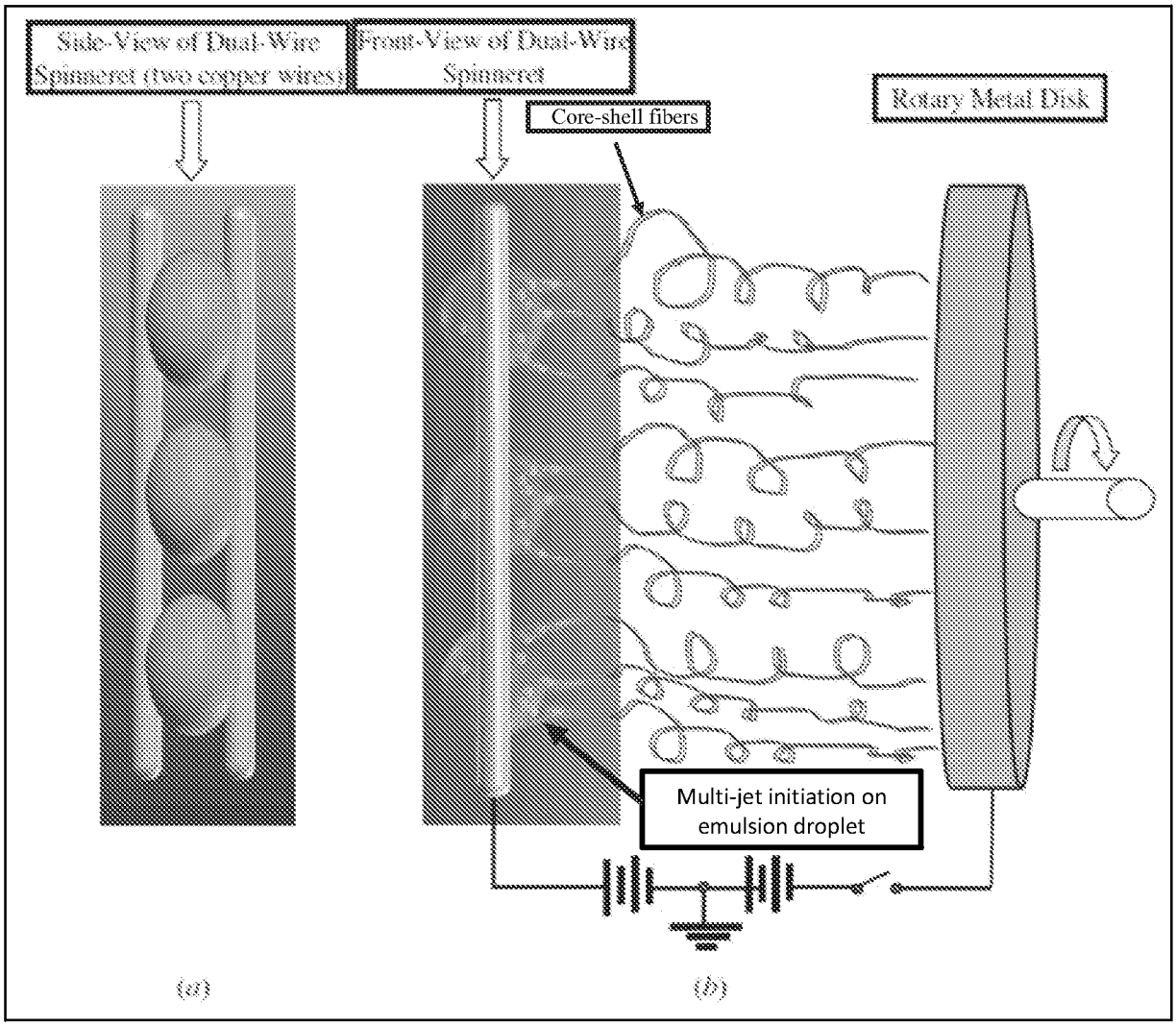
Side-View of Dual-Wire Spinneret (two copper wires)
Front-View of Dual-Wire Spinneret
Core-shell fibers
Rotary Metal Disk
Multi-jet initiation on emulsion droplet
(a)
(b)

FIG. 14

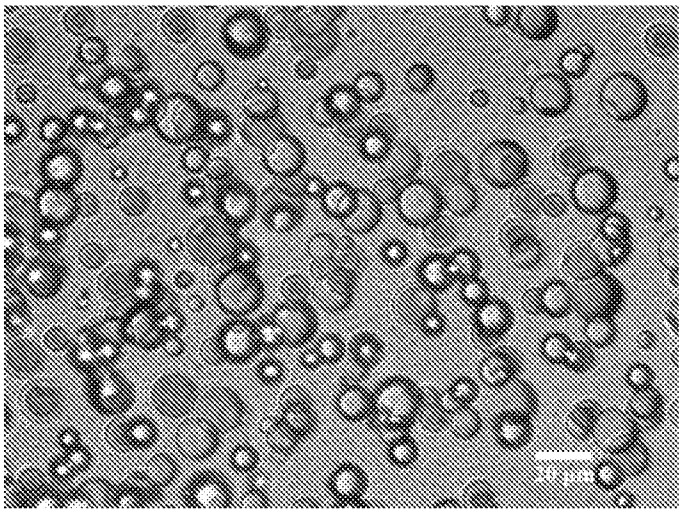

FIG. 15

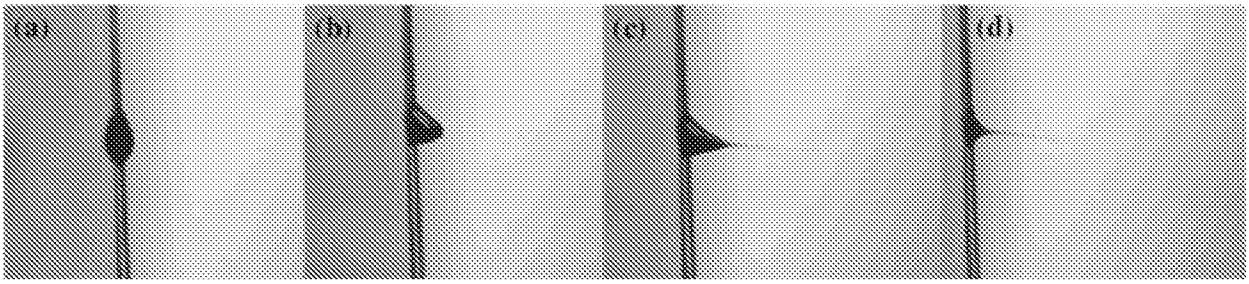

FIG. 16

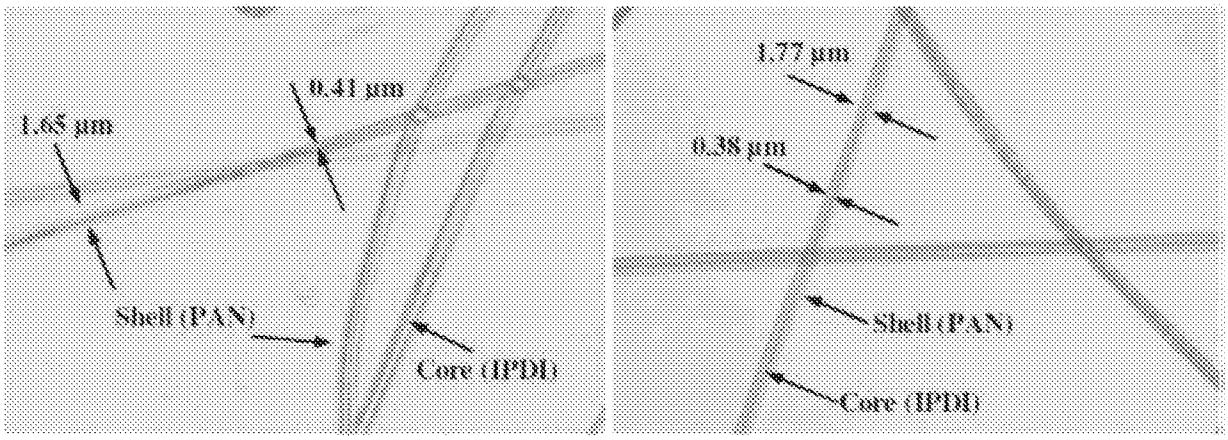

FIG. 17

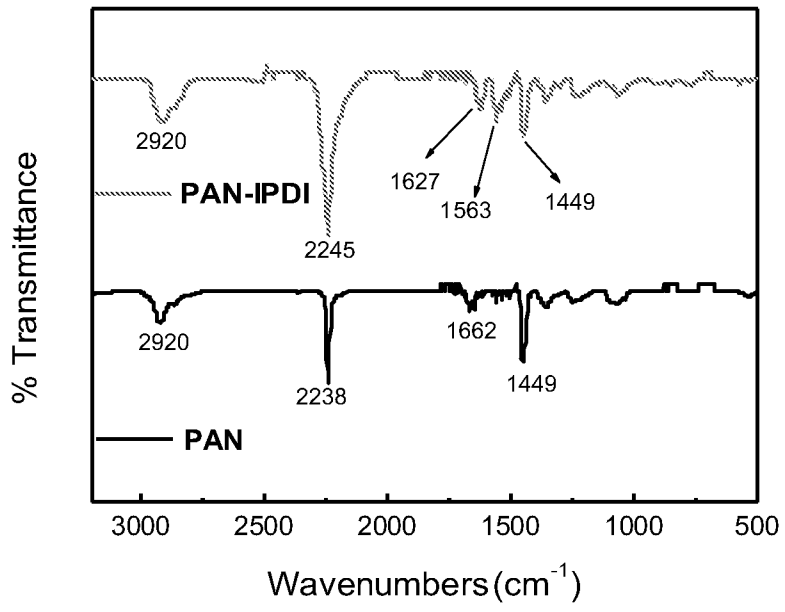

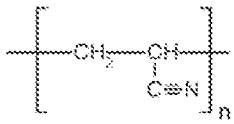

Polyacrylonitrile (PAN)

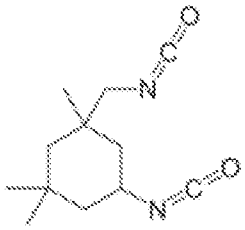

Isophorone diisocyanate (IPDI)

FIG. 18

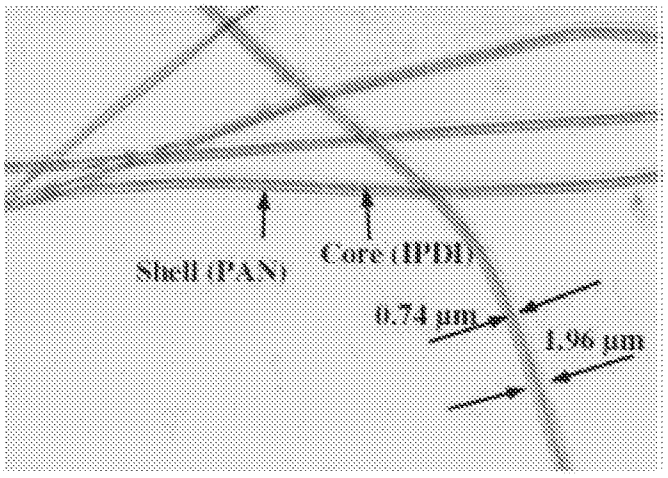
Shell (PAN)
Core (IPDI)
0.74 μm
1.96 μm

FIG. 19

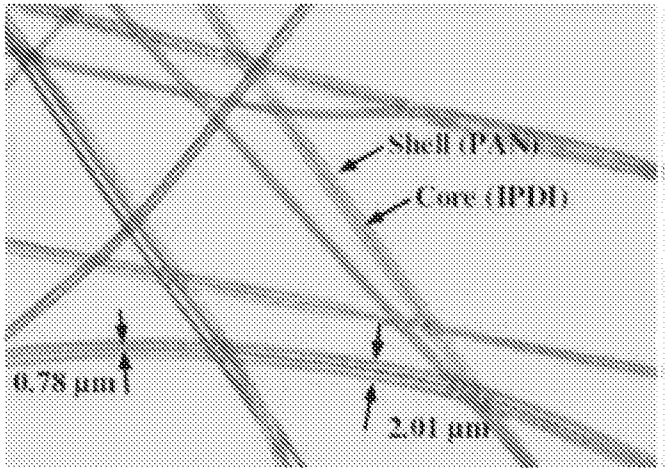
Shell (PAN)
Core (IPDI)
0.78 μm
2.01 μm

FIG. 20